Aristotle University of Thessaloniki
Department of Electrical and Computer Engineering
Telecommunications Department

Gkeralnto Balla
Student ID: 10756

DIPLOMA THESIS

OTFS Modulation in High Mobility Systems: PASS Application and PAPR Reduction

Supervisor: Georgios Karagiannidis, Professor
Co-supervisor: Thrasyvulos Oikonomou, PhD Candidate

Thessaloniki, September 2, 2026

OTFS Modulation in High Mobility Systems:
PASS Application and PAPR Reduction
OTFS Modulation in High Mobility Systems:
PASS Application and PAPR Reduction

Summary

This thesis investigates the Orthogonal Time Frequency Space (OTFS) modulation and its implementation in high mobility telecommunication systems. The OTFS waveform proves to be exceptionally robust in doubly dispersive channels. Through the Symplectic Finite Fourier Transform (ISFFT/SFFT), it spreads the signal energy across both time and frequency, providing substantial diversity against high Doppler conditions.

In the first part, we propose and study the application of OTFS modulation with Pinching Antenna Systems (PASS) for seamless communication with high-speed trains inside tunnels. An analytical mathematical model of the OTFS-PASS channel with fractional delays and Doppler is developed. Asymptotic capacity bounds are derived, and extensive simulations demonstrate the clear superiority of OTFS over OFDM, which fails under high mobility conditions. Finally, we observe that the OTFS waveform exhibits high Peak-to-Average Power Ratio (PAPR), causing distortion due to power amplifier nonlinearities.

To address this problem, the second part analyzes the PAPR of OTFS and proposes a novel Constant Envelope OTFS (CE-OTFS) modulation technique. This technique transfers information to the signal phase, guaranteeing unitary PAPR. The error probability over an AWGN channel is analytically derived, demonstrating the theoretical limits of the method due to phase wrapping phenomena.

Keywords: OTFS, delay-Doppler, wireless communications, high mobility, PAPR, Constant Envelope, Pinching Antennas, PASS, doubly dispersive channels

Abstract

This thesis investigates the Orthogonal Time Frequency Space (OTFS) modulation and its implementation in high mobility telecommunication systems. The OTFS waveform proves to be exceptionally robust in doubly dispersive channels. By utilizing the Symplectic Finite Fourier Transform (ISFFT/SFFT), it spreads the signal's energy across both time and frequency domains, thus providing a massive degree of diversity against high Doppler conditions. However, the waveform suffers from a high Peak-to-Average Power Ratio (PAPR), which leads to signal distortion caused by power amplifier nonlinearities.

In the first part, the application of OTFS modulation with Pinching Antenna Systems (PASS) is proposed and studied, aiming to provide seamless connectivity for high-speed trains inside tunnels. An analytical mathematical model of the OTFS-PASS channel with fractional delays and Doppler shifts is developed. Asymptotic capacity bounds are derived, and extensive simulations demonstrate the clear superiority of OTFS over OFDM, which breaks down under high mobility conditions due to inter-carrier interference. Finally, it is revealed that OTFS suffers from a high Peak-to-Average Power Ratio (PAPR), which leads to signal distortion caused from power amplifier nonlinearities.

To address this issue, the second part of the thesis analyzes the PAPR of OTFS and proposes a novel Constant Envelope OTFS (CE-OTFS) modulation technique. By mapping the information onto the phase of the signal, this technique mathematically guarantees a unitary PAPR. The bit error probability over an AWGN channel is derived analytically, revealing the theoretical performance bounds imposed by the phase wrapping phenomenon.

Keywords: OTFS, delay-Doppler, wireless communications, high mobility, PAPR, Constant Envelope, Pinching Antennas, PASS, doubly dispersive channels

Contents

List of Figures

Chapter 1

Introduction

1.1 General Overview

Modern wireless communication systems, particularly those of the 5th generation (5G) and upcoming 6th generation (6G), are required to meet stringent requirements such as massive data transmission rates, extremely low latency, and uncompromising reliability. However, as these systems are now required to operate in scenarios of exceptionally high mobility (such as high-speed trains and aerial platforms), new challenges emerge. In such environments, the wireless channel exhibits double dispersion (doubly dispersive), as the simultaneous presence of multiple propagation paths (multipath delay) and Doppler shifts destroys the orthogonality of traditional waveforms such as OFDM, causing dramatic performance degradation.

One solution addressing the increased requirements of wireless communication systems is Orthogonal Time-Frequency Space (OTFS) modulation [1], a modern, two-dimensional (2D), modulation technique that ensures near-constant channel gain even in high Doppler environments or at high operating frequencies (e.g., mmWave). OTFS transcends the limitations of the traditional time-frequency domain, placing information symbols in the two-dimensional delay-Doppler domain. Through the Symplectic Finite Fourier Transform (SFFT / ISFFT), OTFS spreads the energy of each symbol across the entire time-frequency domain, achieving full exploitation of channel diversity. As a result, OTFS provides robustness against inter-symbol interference (ISI) and inter-carrier interference (ICI).

In the realm of infrastructure for high mobility systems, Pinching Antenna Systems (PASS) [2], [3] have been proposed as a revolutionary method for providing reliable coverage in challenging environments, such as railway tunnels. The combination of a dielectric waveguide with discrete antennas, when combined with the powerful OTFS waveform, can offer a robust communication framework unaffected by high train speeds.

Nevertheless, OTFS modulation inherits a structural weakness of multi-carrier systems: the high Peak-to-Average Power Ratio (PAPR). The abrupt amplitude fluctuations of the signal drive power amplifiers into their nonlinear operating region, causing severe distortion in the transmitted signal.

1.2 Thesis Contribution

The present thesis aims to overcome the limitations of OTFS modulation and explore its potential in innovative telecommunication architectures. The thesis contribution develops along two main axes:

The first axis focuses on the application of OTFS in PASS systems (OTFS-PASS) for high-speed trains inside tunnels. The channel response is modeled in the presence of fractional delays and Doppler, and the waveform's ability to support high transmission rates is extensively studied. The asymptotic capacity limits of the system are analyzed and the clear superiority of OTFS-PASS over the equivalent OFDM-PASS is confirmed through simulations.

During the above analysis, the problem of high PAPR in the OTFS waveform emerges. For this reason, the second axis of the thesis introduces and theoretically analyzes a new phase modulation technique, Constant Envelope OTFS (CE-OTFS), which mathematically guarantees unitary PAPR. The technique's behavior over an AWGN channel is examined and the error probability is analytically calculated, highlighting the performance limitations due to phase wrapping phenomena.

Chapter 2

General Elements of Wireless Communications

2.1 White Gaussian Noise

Wireless communication systems consist of electronic circuits which in turn are sources of noise. Noise is the main cause of degradation in the operation of wireless communication systems, as it can cause errors in data transmission. In this work, the noise affecting wireless communication systems is considered to be additive white Gaussian noise (Additive White Gaussian Noise - AWGN). White Gaussian noise is a noise model characterized by the normal distribution of its samples. The term "white" refers to the fact that its power spectral density (PSD) is constant over the entire frequency spectrum, i.e.,

$$S_n(f) = \frac{N_0}{2}, \quad \forall f \tag{2.1}$$

Where the quantity $N_0 = -174dBm$ expresses the power of thermal noise. It follows that the auto-correlation function of white Gaussian noise is

$$R_n(\tau) = \frac{N_0}{2}\delta(\tau) \tag{2.2}$$

Therefore, the samples of white Gaussian noise are mutually uncorrelated. Equation (2.1) implies that white Gaussian noise has infinite power, a fact that does not correspond to reality. In practical telecommunication systems, the noise is 'filtered' by some bandpass filter of bandwidth W, with the result that the noise power is finite and equal to

$$P_n = \int_{-\infty}^{\infty} S_n(f)|H(f)|^2 df = N_0 W \tag{2.3}$$

2.2 The Wireless Channel

The wireless channel is the medium through which information transmission takes place and constitutes the mechanism that contributes to the creation of errors generated when information is received at the receiver. Let the transmitted signal be $s(t)$, then its interaction with the channel can be modeled as the convolution with the channel's impulse response $h(t)$

$$r(t) = h(t) * s(t) + n(t) = \int h(\tau)s(t-\tau)\, d\tau + n(t) \tag{2.4}$$

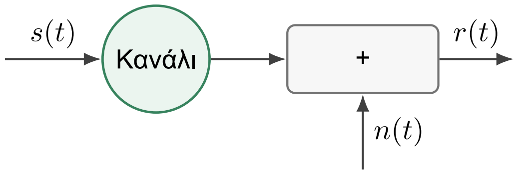

Figure 2.1: General Channel Representation

where the quantity $n(t)$ is white Gaussian noise. Depending on the form of the channel's impulse response and due to additive noise, the signal may undergo distortion in its amplitude and phase, but may also receive interference from previous signals that arrive at the receiver with time delay. These distortions will be studied below.

2.2.1 Additive White Gaussian Noise Channel - AWGN

The simplest modeling of a wireless channel is the Additive White Gaussian Noise (AWGN) channel. In the AWGN channel, the received signal is equal to the transmitted signal, plus a quantity that corresponds to white Gaussian noise. The channel's impulse response is a delta function $h(t) = \delta(t)$ and equation (2.4) becomes

$$r(t) = s(t) + n(t) \tag{2.5}$$

or in discrete form

$$r = s + n \tag{2.6}$$

where $n \sim \mathcal{CN}(0, \sigma_n^2)$. At this point, the signal-to-noise ratio can be defined, which expresses the ratio of the information signal power to the noise power (Signal to Noise Ratio - SNR).

$$\text{SNR} = \frac{P_s}{\sigma_n^2} = \frac{P_s}{N_0 W} \tag{2.7}$$

The SNR of a system is a measure of the quality of the received signal and the greater it is, the smaller will be the number of errors caused by noise. Often the SNR is expressed in terms of symbol energy, i.e.,

$$\text{SNR} = \frac{2E_s}{N_0} \tag{2.8}$$

The expression of the signal-to-noise ratio also provides the spectral efficiency of the channel (spectral efficiency- SE)

$$\text{SE} = \log_2(1 + \text{SNR}) \tag{2.9}$$

2.2.2 Fading Channel

In practical wireless communication systems, a channel can be affected, besides thermal noise at the receiver, by propagation losses that describe the loss of signal power as it is transmitted in free space, by large-scale fading caused by the presence of large fixed obstacles in the signal propagation path and by small-scale fading which are caused by the presence of multiple propagation paths, the relative motion of the terminal and reflections.

The propagation losses are described by the Friis propagation equation:

$$\frac{P_r}{P_t} = G_r G_t \left(\frac{\lambda}{2\pi d}\right)^2 \tag{2.10}$$

where P_r, P_t are the received and transmitted power, G_r, G_t are the gains of the receiving antenna and the transmitting antenna, λ is the wavelength at the operating frequency and d is the distance between transmitter and receiver.

Large-scale fading is usually modeled as a multiplicative stochastic process that varies slowly with time. Their study is outside the scope of this thesis work.

Small-scale fading decisively affects the receiver architecture, the modulation technique and the encoding that will be chosen. As signals propagate through multiple paths, mainly due to reflections, the received signal is a superposition of the information signal which reaches the receiver at different times. As a result, the signal spreads over time (delay spread) and destructive phenomena are caused, such as signal attenuation and intersymbol interference. The time spreading of the signal can be described statistically from the Power Delay Profile (PDP) and hold

$$\bar{\tau} = \frac{\sum_k P(\tau_k)\tau_k}{\sum_k P(\tau_k)} \tag{2.11}$$

$$\bar{\tau^2} = \frac{\sum_k P(\tau_k)\tau_k^2}{\sum_k P(\tau_k)} \tag{2.12}$$

$$\sigma_\tau = \sqrt{\bar{\tau^2} - (\bar{\tau})^2} \tag{2.13}$$

The coherence bandwidth B_c is defined (coherence bandwidth) as a statistical measure of the range of frequencies over which the channel response can be considered constant. A common approximation is given as

$$B_c \approx \frac{1}{5\sigma_\tau} \tag{2.14}$$

When for the baseband signal bandwidth it holds $W < B_c$, then the system is narrowband and the fading is frequency-flat (frequency-flat fading). Otherwise, the system is wideband and the fading is frequency-selective. The received signal is in the general case

$$r(t) = \sum_{k=-\infty}^{\infty} h_k s(t-\tau_k) + n(t) = h_0 s(t) + \sum_{k\in\mathbb{N}^*} h_k s(t-\tau_k) + n(t) \tag{2.15}$$

where the first term describes the useful signal, the second term describes the terms of intersymbol interference (Intersymbol Interference - ISI) and the third term is the noise.

In a fading channel, the fading amplitude $|h_k|$ can be described statistically from various probability distributions. When the strong propagation path does not have line of sight between the transmitter and the receiver (no Line of Sight - nLoS), then the amplitude follows a Rayleigh distribution, with probability density function (PDF)

$$p(r) = \begin{cases} \frac{r}{\sigma^2}\exp(-\frac{r^2}{2\sigma^2}), & 0 \le r < \infty, \\ 0, & r < 0 \end{cases} \tag{2.16}$$

In the case where there is line of sight (Line of Sight - LoS), the amplitude $|h_k|$ follows a Rice distribution with PDF

$$p(r) = \begin{cases} \frac{r}{\sigma^2}\exp\left[-\frac{r^2+A^2}{2\sigma^2}\right] I_0\left(\frac{Ar}{\sigma^2}\right), & r \ge 0 \\ 0, & r < 0 \end{cases} \tag{2.17}$$

$$I_0 \equiv \frac{1}{2\pi}\int_0^{2\pi} \exp[z\cos\theta],\ d\theta \tag{2.18}$$

In the more general case, the fading amplitude is described statistically from the Nakagami-m distribution, with PDF

$$p(r) = \frac{2m^m r^{2m-1}}{\Omega^m \Gamma(m)} \exp\left(-\frac{mr^2}{\Omega}\right), \quad r \geq 0 \tag{2.19}$$

In the case where $m = 1$, the Nakagami-m distribution coincides with the Rayleigh distribution.

In a fading channel, the signal-to-noise ratio is generalized and includes any interference, resulting in the definition of the signal-to-interference-plus-noise ratio (Signal to Interference plus Noise Ratio - SINR)

$$\text{SINR} = \frac{P_{s_0}}{P_{ISI} + \sigma_n^2} \tag{2.20}$$

In the case where there is no intersymbol interference, then the signal-to-noise ratio (2.7) becomes

$$\text{SNR} = \frac{|h_0|^2 P_s}{\sigma_n^2} \tag{2.21}$$

The SNR, that is, is now a stochastic process which is described by the statistical distribution of the fading amplitude. A better metric for system evaluation is the Average Signal to Noise Ratio (ASNR) which is calculated as

$$\text{ASNR} = E[SNR] \tag{2.22}$$

2.2.3 Doubly-Spread Channel

In channels where there is relative mobility between the transmitter and receiver, the received signal suffers additionally from Doppler phenomena. The relative motion between transmitter and receiver causes frequency shifts of the information signal which, in systems where modulation is done in the frequency domain, cause inter-carrier interference phenomena (Inter Carrier Interference - ICI). The coherence time T_c (Coherence Time) is defined as a statistical measure of the time duration over which the channel's impulse response remains constant. A common approximation is given as

$$T_c \approx \frac{0.423}{f_m} \tag{2.23}$$

where f_m is the maximum Doppler spread (Doppler spread).

2.3 Digital Modulation

In modern telecommunication systems, the information signal is usually a sequence of binary information digits (bits). Each bit or group of bits is mapped to some waveform, transmitted through the channel and detected by the receiver. The simplest case of digital modulation is M-PAM modulation (M-ary Pulse Amplitude Modulation). In this case, the information bits are divided into groups of $\log_2 M$, and mapped to amplitude levels that modulate some baseband pulse $g(t)$. A graphical representation of the 4-PAM modulation is shown, as an example, in Figure 2.2. The transmission pulse

Figure 2.2: 4-PAM Modulation

that will be used henceforth in this work is the rectangular pulse of duration T:

$$g(t) = \text{rect}(t/T) = \begin{cases} 1, & |t| \leq T \\ 0, & \text{elsewhere} \end{cases} \tag{2.24}$$

while other pulses are often used, such as the Raised Cosine pulse family and others. In the frequency domain, the rectangular pulse has the representation

$$G(f) = T\text{sinc}(fT) \tag{2.25}$$

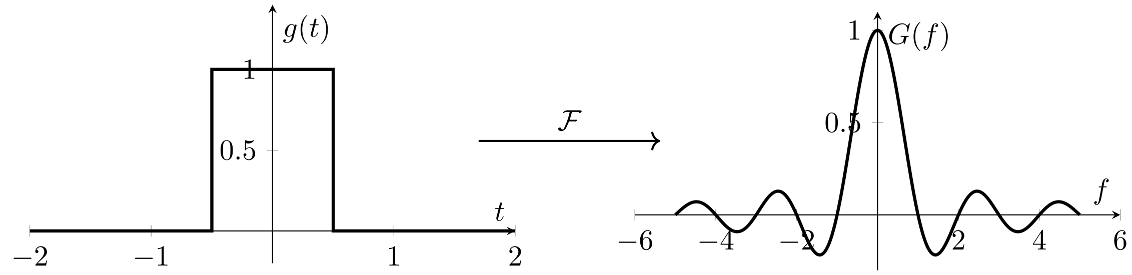

Figure 2.3: The rectangular pulse in the time domain (left) and frequency domain (right).

Each amplitude level in M-PAM modulation corresponds to a symbol and is displayed as a point on the plane. The set of symbols is called a constellation, while the number of symbols within the constellation is called the modulation order. The need to transmit a larger volume of information reliably and with good spectral efficiency leads to the use of constellations of higher dimension. While there are many types of constellations (Phase Shift Keying- PSK, Frequency Shift Keying - FSK, etc.), particular interest for this work is shown by M-QAM constellations (Quadrature Amplitude Modulation). QAM constellations can be decomposed into two orthogonal components, In-Phase (I) and Quadrature (Q), each of which corresponds to symbols of $\sqrt{M}$-PAM constellations.

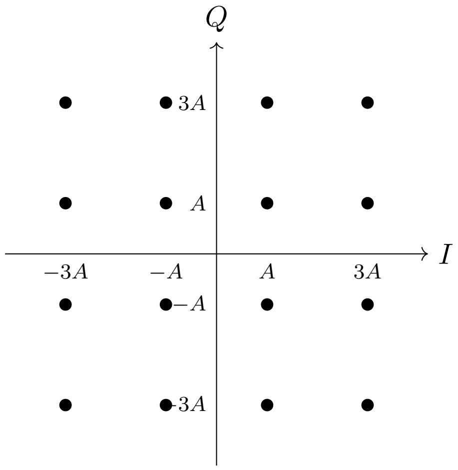

Figure 2.4: 16-QAM Modulation

Let $\{a_k\}_{k=-\infty}^{\infty}$, $a_k \in \mathbb{C}$ form a sequence of symbols from a two-dimensional constellation, such as 16-QAM (Figure 2.4). Then the baseband signal that is transmitted is

$$s(t) = \sum_{k=-\infty}^{\infty} a_k g(t - kT) \tag{2.26}$$

and is received according to equation (2.4). The received signal then enters a demodulator, which reverses the modulation process and produces at its output an estimate of the transmitted sequence plus the additive noise, that is the sequence $\{r_k\}_{k=-\infty}^{\infty}$, $r_k = a_k + n_k$. Optimal detection is performed by the maximum a posteriori probability detector, which makes decisions according to

$$\hat{a_k} = \arg\max_{\{a_k\}}\{\Pr(a_k|r_k)\} = \arg\min_{\{a_k\}}\{\|r_k - a_k\|^2\} \tag{2.27}$$

provided that every symbol of the constellations studied is equally likely. From the detection of transmitted symbols, a very useful metric emerges for evaluating wireless communication systems, called Bit Error Rate (BER). The BER is calculated through the statistics of the model and for the M-PAM constellation is approximated as

$$P_b \approx \frac{2(M-1)}{M\log_2 M} Q\left(\sqrt{\frac{6\mathcal{E}_b \log_2 M}{(M^2-1)N_0}}\right) \tag{2.28}$$

where the $Q(\cdot)$ is the Gaussian Q-function, with

$$Q(x) = \frac{1}{\sqrt{2\pi}}\int_x^{\infty} e^{-\frac{t^2}{2}}\, dt \tag{2.29}$$

Similar expressions, whether exact or approximate, are calculated for other types of constellations.

Chapter 3

OTFS Modulation

3.1 Multi-Carrier Modulation

In environments with multiple propagation paths of the same signal, the channel exhibits frequency-selective behavior. For reliable information transmission, the baseband information signal should have a bandwidth smaller than the coherent bandwidth and is typically chosen according to the empirical rule

$$W \leq 0.1 B_c \tag{3.1}$$

The imposition of narrow bandwidth ensures that each channel experiences almost flat fading, limiting the effects of channel frequency selectivity. However, the use of a single carrier leads to low spectral efficiency and does not effectively utilize the available bandwidth. For this reason, the bandwidth is divided into narrower bands that satisfy the (3.1), each of which corresponds to a subcarrier. By choosing the spacing between subcarriers appropriately, orthogonality between them is achieved, allowing simultaneous transmission of multiple data streams without interference. The most common multi-carrier modulation technique is Orthogonal Frequency Division Multiplexing (OFDM).

3.1.1 Orthogonal Frequency Division Multiplexing (OFDM)

In OFDM modulation, transmission occurs at the block level. Let there be a sequence of N symbols of a constellation $\mathcal{A}$, $\{X[n]\}_{n=0}^{N-1}$, $X[n] \in \mathcal{A}$. The transmission of the sequence occurs according to

$$s(t) = \sum_{n=0}^{N-1} X[n] g_n(t) \tag{3.2}$$

To achieve orthogonality, rectangular pulses are chosen, with duration T_s

$$g_n(t) = \begin{cases} \frac{1}{\sqrt{T_s}} \exp\left(j2\pi n \frac{t}{T_s}\right), & 0 < t \leq T_s \\ 0, & elsewhere \end{cases} \tag{3.3}$$

and therefore

$$s(t) = \frac{1}{\sqrt{T_s}} \sum_{n=0}^{N-1} X[n] e^{j2\pi n \frac{t}{T_s}} \tag{3.4}$$

It is worth noting that each symbol c_n is transmitted with a rectangular pulse, all of which are displayed in the frequency domain as functions $G_n(f) = \sqrt{T_s}\mathrm{sinc}((f - \frac{n}{T_s})T_s)$, with the spacing between two consecutive carriers being $\Delta f \equiv \frac{1}{T_s}$ (Figure 3.1).

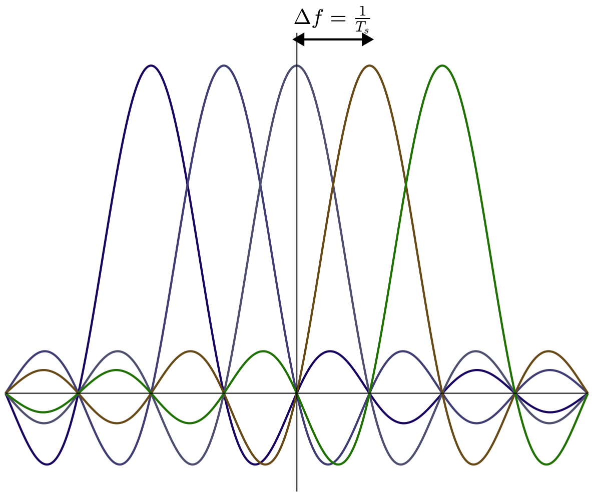

Figure 3.1: OFDM Subcarriers

After sampling at a rate $f_s = \frac{N}{T_s} = W_{tot}$, the samples are obtained

$$s_k = \frac{1}{\sqrt{T_s}} \sum_{n=0}^{N-1} X[n] e^{j2\pi \frac{n}{N}} \tag{3.5}$$

At this point, it appears that the generation of the OFDM symbol in the discrete time domain is equivalent to applying an Inverse Discrete Fourier Transform (IDFT) to the subcarrier symbols. The latter is easily implementable at the hardware level through the (Inverse) Fast Fourier Transform (FFT/IFFT) algorithm, and for this reason, the OFDM technique is the most widely used modulation technique in modern telecommunications systems.

The detection of symbols at the receiver is performed using the Discrete Fourier Transform (FFT) on the received sequence. The effect of the channel is written, in discrete form, as

$$r[n] = h[n] * s[n] + w[n] = \sum_k h[k] s[n-k] + w[n] \tag{3.6}$$

where $w[n] \sim \mathcal{CN}(0, \sigma_w^2)$ is the additive noise. By applying a cyclic prefix (cyclic prefix - CP) to the sequence transmitted from the transmitter, the property of multiplication in the discrete frequency domain is exploited. That is

$$r[n] = \sum_k h[k] \hat{s}[n-k] + w[n] = \sum_k h[k] s[(n-k)_N] + w[n] = h[n] \circledast s[n] + w[n] \tag{3.7}$$

where $(\cdot)_N$ denotes the remainder of division by N (mod$N$) and $\circledast$ is the circular convolution. In the frequency domain, the (3.7) becomes

$$R[i] = \text{DFT}\{h[n] \circledast s[n] + w[n]\} = H[i]X[i] + W[i],\, i = 0, ..., N-1 \tag{3.8}$$

where $H[i]$ is the channel response at the frequency of the i-th subcarrier and $W[i] \sim \mathcal{CN}(0, \sigma_w^2)$ is the additive noise. Channel equalization, therefore, only requires dividing the received symbol of each subcarrier by the corresponding channel gain at that frequency. The signal-to-noise ratio and spectral efficiency of OFDM are

$$\gamma_i = \frac{P_i |H[i]|^2}{\sigma_w^2} \tag{3.9}$$

$$\text{SE} = \frac{1}{B} \sum_{i=0}^{N-1} \Delta f \log_2(1+\gamma_i) = \frac{1}{N} \sum_{i=0}^{N-1} \log_2(1+\gamma_i) \tag{3.10}$$

3.2 OTFS (Orthogonal Time-Frequency Space) Modulation

3.2.1 The Delay-Doppler Domain

In a typical wireless channel between a transmitter and a receiver, the form of the received signal is determined by a small number of strong propagation paths [4]. Each path is characterized by the path delay, that is, the time it takes for the signal to reach the receiver through the path, and by the Doppler shift, which is the frequency shift due to the relative motion between the transmitter, reflector, and receiver. Such a channel is shown in Figure 3.2. As mentioned in subsection 2.2.3, such channels

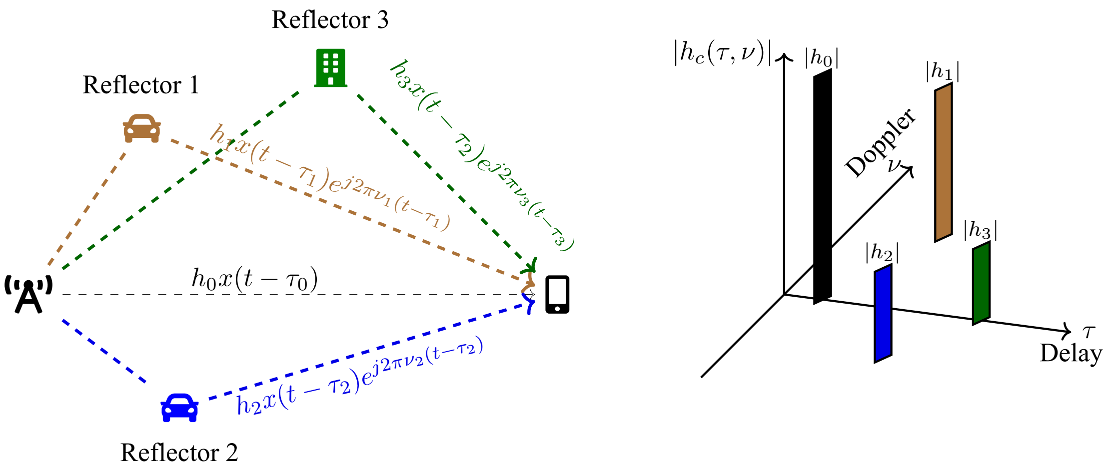

Figure 3.2: Channel representation in the delay-Doppler domain. Each propagation path corresponds to a discrete component of the channel, characterized by specific delay, Doppler shift, and gain. In most wireless environments, the number of dominant paths is limited, resulting in the channel having a sparse representation in the delay-Doppler domain. This property is exploited by OTFS modulation for more effective channel estimation and compensation.

exhibit double spread (doubly spread channel). These channels are described by the spreading function in the delay-Doppler domain (delay-Doppler (DD) spreading function) $h_c(\tau,\nu)$, where $\tau \in \mathbb{R}$ and $\nu \in \mathbb{R}$ are the delay and Doppler variables, respectively

$$h_c(\tau,\nu) = \sum_{i=1}^{P} h_i \delta(\tau-\tau_i)\delta(\nu-\nu_i) \tag{3.11}$$

where P is the number of propagation paths and $\delta(\cdot)$ is the Dirac-delta function. The noise-free signal received in the continuous time domain, when the signal $x(t)$ is transmitted, will be

$$y(t) = \int\int h_c(\tau,\nu)x(t-\tau)e^{j2\pi\nu(t-\tau)}\, d\tau d\nu \tag{3.12}$$

which using the (3.11) becomes

$$y(t) = \sum_{i=1}^{P} h_i x(t-\tau_i)e^{j2\pi\nu_i(t-\tau_i)} \tag{3.13}$$

In other words, the channel representation in the delay-Doppler domain indicates that its significant components are concentrated in a small number of positions (τ_i, ν_i). This observation is the main motivation for OTFS modulation, which places information in the delay-Doppler domain to exploit the channel structure.

3.2.2 Modulation via the Time-Frequency Domain

Consider a telecommunications system which transmits information occupying a bandwidth W, divided into M subcarriers each of which has a frequency range Δf, such that $W = M\Delta f$, and transmits them over N time slots of duration T, such that $T_{tot} = NT$. In the delay-Doppler domain, a discrete, periodic grid with periods (N, M), denoted Λ, is defined and samples the delay and Doppler dimensions, respectively, at integer multiples of $\Delta\nu = \frac{1}{NT}$ and $\Delta\tau = \frac{1}{M\Delta f}$, that is

$$\Lambda = \{(k\Delta\nu, l\Delta\tau) : k, l \in \mathbb{Z}\} \tag{3.14}$$

then the desired transmission sequence, consisting of symbols of a constellation $\mathcal{A}$, is placed at grid points with indices $k = 0, ..., N-1\,, l = 0, ..., M-1$, that is $x[k, l] \in \mathcal{A}$. These symbols are repeated periodically with periods (N, M), creating the sequence $x_p[k, l]$. Using the Inverse Symplectic Finite Fourier Transform (ISFFT), the symbols $x_p[k, l]$ are converted to symbols in the time-frequency domain (time-frequency - TF) according to

$$X_p[n, m] = \frac{1}{\sqrt{NM}} \sum_{k=0}^{N-1} \sum_{l=0}^{M-1} x_p[k, l] e^{-j2\pi(\frac{ml}{M} - \frac{nk}{N})} \tag{3.15}$$

for $n = 0, ..., N-1$ and $m = 0, ..., M-1$. The symbols $X_p[n, m]$, therefore, are placed at the points of the dual grid, in the time-frequency domain, $\Lambda^{\perp}$, which samples the time and frequency dimensions, respectively, at integer multiples of T, Δf, that is

$$\Lambda^{\perp} = \{(nT, m\Delta f) : n, m \in \mathbb{Z}\} \tag{3.16}$$

The sequence of symbols finally transmitted is

$$X[n, m] = W_{tx}[n, m] X_p[n, m] = W_{tx}[n, m] \text{ISFFT}(x_p[k, l]) \tag{3.17}$$

Where $W_{tx}[n, m]$ with $\sum_{n,m} \|W_{tx}[n, m]\|^2 < \infty$ is some windowing function. Subsequently, the transmitted signal in the continuous time domain is given by the Heisenberg transform of the symbol sequence $X[n, m]$:

$$s(t) = \sum_{n=0}^{N-1} \sum_{m=0}^{M-1} X[n, m] g_{tx}(t - nT) e^{j2\pi m\Delta f(t-nT)} \tag{3.18}$$

Equation (3.18) shows that OTFS is not a new waveform at the physical layer, but a preprocessing of symbols before transmission via OFDM-type waveforms. After the transmitted signal undergoes the effect of the channel, the receiver receives:

$$r(t) = \int_{\tau} \int_{\nu} h_c(\tau, \nu) s(t - \tau) e^{j2\pi\nu(t-\tau)}\, d\nu d\tau + v(t) \tag{3.19}$$

where $v(t)$ denotes the additive noise. The first step the demodulator applies is the computation of the cross-correlation function in the delay-Doppler domain (cross-ambiguity function). The function is denoted as $A_{g_{rx},r}(\tau,\nu)$ and is calculated as

$$A_{g_{rx},r}(\tau,\nu) \triangleq \int g^*_{rx}(t-\tau)r(t)e^{-j2\pi\nu(t-\tau)}\,dt \tag{3.20}$$

The cross-ambiguity function is sampled at integer multiples of time T and frequency Δf and the sequence is obtained

$$\hat{Y}[n,m] = A_{g_{rx},r}(\tau,\nu)|_{\tau=nT,\nu=m\Delta f} \tag{3.21}$$

The transformation of the received, continuous signal $r(t)$ into a two-dimensional symbol sequence $\hat{Y}[n,m]$ is referred to in the literature as the discrete Wigner transform. Subsequently, a windowing function is applied to the sequence, typically similar to the one described in (3.17), such that

$$\hat{Y}_W[n,m] = W_{rx}[n,m]\hat{Y}[n,m] \tag{3.22}$$

The sequence $\hat{Y}_W[n,m]$ is periodized and passes through the Symplectic Finite Fourier Transform (SFFT), which is the inverse transform of the ISFFT of (3.15)

$$\hat{Y}_p[n,m] = \sum_{n'=-\infty}^{\infty}\sum_{m'=-\infty}^{\infty}\hat{Y}_W[n-n'N, m-m'M] \tag{3.23}$$

$$\hat{y}_p[k,l] = \text{SFFT}(\hat{Y}_p[n,m]) \tag{3.24}$$

Finally, the output of the demodulated symbols is obtained as $\hat{y}[k,l] = \hat{y}_p[k,l]$, $k=0,...,N-1, l=0,...,M-1$. In other words, it holds

$$\hat{y}[k,l] = \frac{1}{\sqrt{NM}}\sum_{n=0}^{N-1}\sum_{m=0}^{M-1}\hat{Y}[n,m]e^{j2\pi(\frac{ml}{M}-\frac{nk}{N})} \tag{3.25}$$

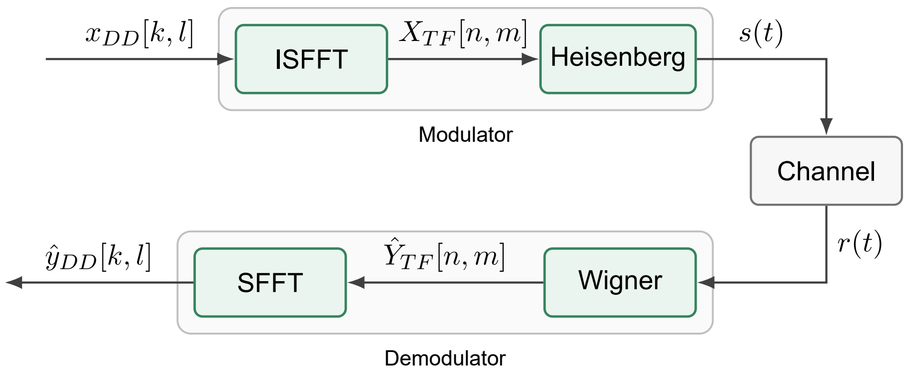

Figure 3.3: Stages of OTFS modulation and demodulation. The symbols in the delay-Doppler domain are first transformed to the time-frequency domain via ISFFT and then to the continuous time domain via the Heisenberg transform. At the receiver, the inverse Wigner and SFFT operations are applied to recover the symbols in the delay-Doppler domain.

Suppose that the transmit and receive pulses satisfy the criterion of bi-orthogonality in the delay-Doppler domain

$$A_{g_{rx}g_{tx}} = \int e^{-j2\pi m\Delta f(t-nT)}g^*_{rx}(t-nT)g_{tx}(t)\,dt = \delta[m]\delta[n] \tag{3.26}$$

Then the periodic convolution of the channel with the windowing filters is given as

$$h_w(\tau,\nu) = \int\int e^{-j2\pi\nu'\tau'}h_c(\tau',\nu')w(\nu-\nu',\tau-\tau')\,d\tau' d\nu' \tag{3.27}$$

Where the function $w(\nu, \tau)$ is periodic with periods $(N\Delta\nu, M\Delta\tau)$ in the delay and Doppler respectively, and is calculated as

$$w(\nu, \tau) = \sum_{n=-\infty}^{\infty} \sum_{m=-\infty}^{\infty} e^{-j2\pi(\nu nT - \tau m\Delta f)} W[n, m] \tag{3.28}$$

The input-output relationship of OTFS modulation is, ultimately

$$\hat{y}_p[k, l] = \frac{1}{NM} \sum_{k'=0}^{N-1} \sum_{l'=0}^{M-1} h_w(k'\Delta\nu, l'\Delta\tau) x_p[k - k', l - l'] + v(k, l) \tag{3.29}$$

where $v(k, l)$ is the additive noise[1].

In the case where $W_{tx}[n, m] = W_{rx}[n, m] = 1$, $n = 0, ..., N - 1, m = 0, ..., M - 1$ the (3.28) becomes

$$w(\nu, \tau) = \sum_{n=0}^{N-1} \sum_{m=0}^{M-1} e^{-j2\pi(\nu nT - \tau m\Delta f)} \tag{3.30}$$

Using the (3.11) in (3.27) we get

$$h_w(\nu, \tau) = \sum_{i=1}^{P} h_i e^{-j2\pi\nu_i\tau_i} w(\nu - \nu_i, \tau - \tau_i) \tag{3.31}$$

and finally the (3.29) becomes

$$\begin{aligned} \hat{y}_p[k, l] = \frac{1}{NM} \sum_{i=1}^{P} \sum_{k'=0}^{N-1} \sum_{l'=0}^{M-1} h_i e^{-j2\pi\nu_i\tau_i} \sum_{n=0}^{N-1} e^{-j2\pi nT(k'\Delta\nu - \nu_i)} \sum_{m=0}^{M-1} e^{j2\pi m\Delta f(l'\Delta\tau - \tau_i)} \\ \times x_p[k - k', l - l'] + v[k, l] \end{aligned} \tag{3.32}$$

It is assumed that the delays and Dopplers of the paths correspond to points of the lattice Λ, that is

$$\nu_i = \frac{k_{\nu_i}}{NT}, \qquad \tau_i = \frac{l_{\tau_i}}{M\Delta f} \tag{3.33}$$

Then for the two sums at the end of the (3.32) it will hold

$$\sum_{n=0}^{N-1} e^{-j2\pi nT(k'\Delta\nu - \nu_i)} \sum_{m=0}^{M-1} e^{j2\pi m\Delta f(l'\Delta\tau - \tau_i)} = \sum_{n=0}^{N-1} e^{-j2\pi\frac{n}{N}(k' - k_{\nu_i})} \sum_{m=0}^{M-1} e^{j2\pi\frac{m}{M}(l' - l_{\tau_i})} \tag{3.34}$$

The terms of the sums with respect to n, m in (3.34) are recognized as Dirichlet kernels, which are zero at all lattice points except those corresponding to the delays and Doppler shifts of the paths. The Dirichlet kernels are defined as

$$\mathcal{F}(\tau, \tau_i) \triangleq \sum_{m=0}^{M-1} e^{j2\pi(\tau - \tau_i)m\Delta f} = \frac{e^{j2\pi(\tau - \tau_i)M\Delta f} - 1}{e^{j2\pi(\tau - \tau_i)\Delta f} - 1} \tag{3.35}$$

$$\mathcal{G}(\nu, \nu_i) \triangleq \sum_{n=0}^{N-1} e^{-j2\pi(\nu - \nu_i)nT} = \frac{e^{-j2\pi(\nu - \nu_i)NT} - 1}{e^{-j2\pi(\nu - \nu_i)NT} - 1} \tag{3.36}$$

[1]The noise samples undergo unitary transformations, that is, their energy does not change. Therefore, the statistics of the samples remain invariant during the demodulation process

and are evaluated at the points $\tau = \frac{l'}{M\Delta f}$, $\nu = \frac{k'}{NT}$, respectively. For the Dirichlet kernel $\mathcal{F}(\frac{l'}{M\Delta f}, \tau_i)$ it will hold

$$\mathcal{F}(\frac{l'}{M\Delta f}, \tau_i) = \frac{e^{j2\pi(l'-l_{\tau_i})} - 1}{e^{j\frac{2\pi}{M}(l'-l_{\tau_i})} - 1} = \begin{cases} M, & (l'-l_{\tau_i})_M = 0 \\ 0, & \text{otherwise} \end{cases} \tag{3.37}$$

Similarly, the Dirichlet kernel $\mathcal{G}(\frac{k'}{NT}, \nu_i)$ is computed and the final input-output relationship in the delay-Doppler domain is formulated as

$$y[k,l] = \sum_{i=1}^{P} h_i e^{-j2\pi\nu_i\tau_i} x[(k-k_{\nu_i})_N, (l-l_{\tau_i})_M] + v[k,l] \tag{3.38}$$

This relationship describes the simplest case where the delays and Dopplers are fully aligned with

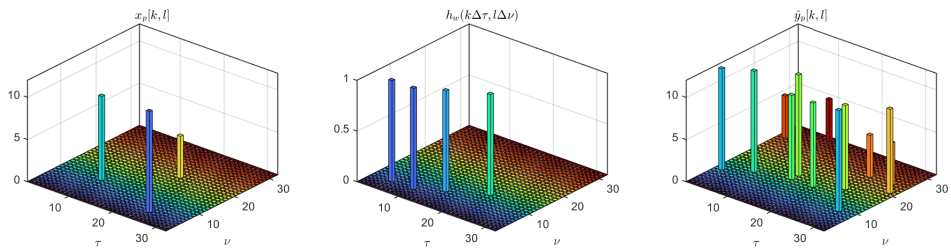

Figure 3.4: OTFS input-output relationship. On the left are the modulated symbols in the delay-Doppler domain, in the middle is the channel representation in the delay-Doppler domain, and on the right is the demodulator output in the delay-Doppler domain

the discrete lattice Λ. In other cases, fractional delays and Dopplers appear, leading to energy leakage from one symbol into neighboring lattice cells (Inter-Delay and Inter-Doppler Interference). The case of non-integer delays and Dopplers is studied in Chapter 4.

Chapter 4

OTFS in PASS Systems

This chapter presents Pinching Antenna (PASS) systems [2], [5] and analyzes the way in which the resulting channel structure can be exploited for the design of OTFS waveforms. The application of such systems aims to ensure reliable communications in environments with high mobility, such as, for example, railway tunnels.

4.1 Pinching Antenna Systems (PASS)

PASS systems constitute an innovative approach in the field of flexible-antenna technologies, with the capability of significant upgrade of wireless communications. Structurally, they consist of two main parts: a dielectric waveguide and an array of pinching antennas (Pinching Antennas - PAs) [3]. The

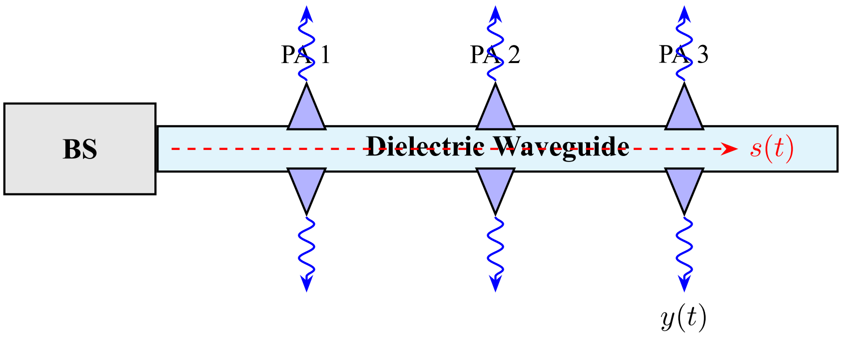

Figure 4.1: Typical structure of a PASS system

dielectric waveguide functions as a transmission medium, ensuring the propagation of the electromagnetic wave over long distances with exceptionally low losses. The PA antennas are placed along the waveguide and allow the radiation of the signal into free space. Their fundamental innovation lies in the fact that the dynamic control of the number and the position of active PA antennas enables the effective handling of fading both at small and large scales. Additionally, selective activation of exclusively the antennas that optimize the link with each respective user becomes possible, thus ensuring continuous connectivity with a strong line-of-sight (Line-of-Sight - LoS) component.

For the purposes of this work, it is henceforth assumed that the waveguide is ideal (lossless), the PA antennas are distributed at fixed positions and their activation is performed in a discrete manner. Under these conditions, the received signal from the transmission of a specific PA antenna is described by the equation:

$$y(t) = \sqrt{P_m}\frac{\sqrt{\eta}}{r_m} \exp\left(-j\frac{2\pi}{\lambda}r_m\right) \times \exp\left(-j\frac{2\pi}{\lambda}n_{eff}d_m\right) s(t) \tag{4.1}$$

where $y(t)$ and $s(t)$ are the received and transmitted signals, respectively. The parameter P_m represents the transmission power of the antenna, while r_m and d_m are the distance between the antenna and the receiver, and the distance of the antenna from the feed point of the waveguide, respectively. Furthermore, $\eta = \frac{c^2}{16\pi^2 f_c^2}$ is a constant related to propagation in free space, λ is the wavelength at the operating frequency f_c, and n_{eff} is the effective relative dielectric constant of the waveguide.

4.2 OTFS-PASS

Particular interest is shown in the use of the OTFS waveform in PASS systems. The case of application of PASS systems under conditions where the receiver moves at high speed relative to the transmitter will be studied. Specifically, the OTFS waveform will be designed so as to serve a moving train inside a tunnel that is equipped with a PASS system.

4.2.1 System Modeling

Consider a downlink communication system consisting of a base station (base station - BS) that feeds a dielectric waveguide equipped with P PAs belonging to the set $\mathcal{P} = \{1, ..., P\}$. Considering a three-dimensional Cartesian coordinate system, the waveguide is placed, without loss of generality, parallel to the x axis and at height H. The waveguide has length L that coincides with the length of the tunnel. The PAs are placed uniformly along the waveguide and their positions are given as $\psi_i^P = (x_i, 0, H)$, with $x_i = \frac{iL}{P+1}, i = 1, ..., P$. The base station is placed at the position $\psi_0 = (0, 0, H)$. The train moves along the x axis, that is, below the waveguide with constant velocity $\vec{\mathbf{v}} = (v_x, 0, 0)$. Its position is given at each time instant as $\psi_u = (x_u, 0, 0)$. According to equation (4.1) the channel between the train and the i-th antenna is described by

$$h_i = \frac{\sqrt{\eta} e^{-j\frac{2\pi}{\lambda}\|\psi_u - \psi_i^P\|}}{\|\psi_u - \psi_i^P\|} \tag{4.2}$$

The signal that arrives at each antenna is a copy of the signal transmitted by the base station, phase-shifted. The effect of propagation through the dielectric waveguide is given as

$$h_{0,i} = e^{-j\frac{2\pi}{\lambda}n_{eff}\|\psi_0 - \psi_i^P\|} \tag{4.3}$$

The base station transmits a signal $s(t)$ with bandwidth B and total transmission time T_{tot}. It is assumed that the transmission speed is significantly higher than the speed of the train, therefore during the transmission of the signal the channel can be considered invariant. Furthermore, the base station transmits with total power P_t which is distributed uniformly among the antennas and the available time-frequency resources.

The channel is described in the general case by the impulse response

$$h(t, \tau) = \sum_{i=1}^{P} h_{0,i} h_i e^{-j2\pi\nu_i t} \delta(\tau - \tau_i) \tag{4.4}$$

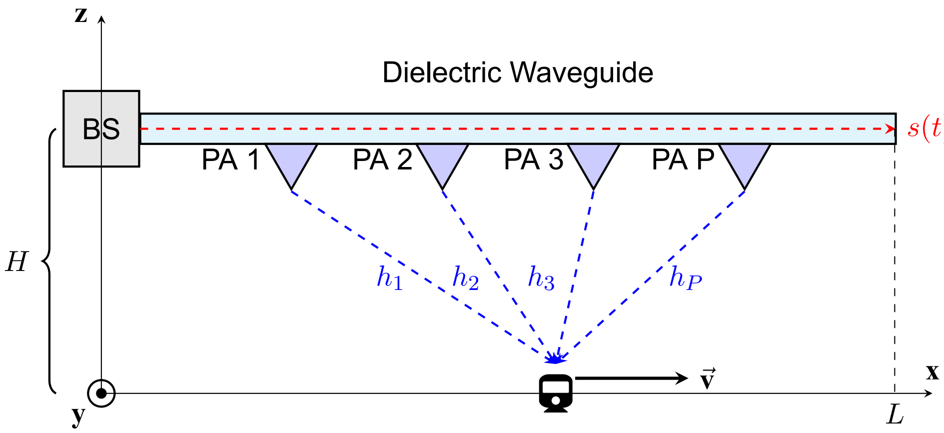

Figure 4.2: Representation of the OTFS-PASS system

where $\tau_i = \frac{\|\psi_u - \psi_i^P\|}{c} + \frac{n_{eff}\|\psi_0 - \psi_i^P\|}{c}$ is the propagation delay of each path and $\nu_i = -\frac{1}{\lambda}\vec{\mathbf{v}} \cdot \frac{\vec{\mathbf{R}}}{\|\vec{\mathbf{R}}\|}$, $\vec{\mathbf{R}} = \psi_u - \psi_i^P$ is the frequency shift due to the Doppler phenomenon resulting from the relative velocity between transmitter and receiver. Then, the received signal at the receiver will be

$$r(t) = \sqrt{\rho} \int h(t,\tau)s(t-\tau)d\tau + n(t) = \sqrt{\rho} \sum_{i=1}^{P} h_{0,i} h_i e^{-j2\pi\nu_i t} s(t-\tau_i) + n(t) \quad (4.5)$$

where $\rho = \frac{P_t}{P}$ and $n(t)$ is additive noise. The channel exhibits double dispersion and is characterized by the maximum time dispersion (delay spread), $\max_i \tau_i - \min_i \tau_i$, and the maximum Doppler dispersion (Doppler spread), $\max_i \nu_i - \min_i \nu_i$. In PASS systems within railway tunnels, due to large distances and velocities, time dispersion and Doppler spread can take large values, making the channel highly frequency-selective and time-varying. Thus, the need arises for the use of some multicarrier waveform that can ensure reliable communication in environments with double dispersion, such as the OTFS waveform.

4.2.2 OTFS Waveform Analysis

A. Input-Output Relationship

The channel of (4.4) is described in the delay-Doppler domain by the scattering function

$$h_c(\tau,\nu) = \sum_{i=1}^{P} h_{0,i} h_i \delta(\tau - \tau_i)\delta(\nu - \nu_i) \quad (4.6)$$

$N \times M$ symbols are selected from a normalized constellation $\mathcal{A}$ and placed in a delay-Doppler domain grid of size $N \times M$, that is $x[k,l] \in \mathcal{A}, k = 0, 1, ..., N-1, l = 0, 1, ..., M-1$. The bandwidth of the system will be $B = M\Delta f$ while the total transmission time will be $T_{tot} = NT$, such that $T = 1/\Delta f$. The quantity Δf, that is, defines both the total bandwidth and the total transmission time. Its selection is made such that $\tau_{\max} \ll T$ and $\nu_{\max} \ll \Delta f$. The latter conditions ensure that the bandwidth of a subcarrier and the transmission duration of a time slot lie within the coherence bandwidth and coherence time, respectively. The dimensions of the grid determine the resolution of the delay-Doppler domain, $\Delta\tau = \frac{1}{M\Delta f}$ and $\Delta\nu = \frac{1}{NT}$ respectively.

Equation (3.29) shows that the input-output relationship of the channel can be written in the form

$$\hat{x}[k,l] = \sqrt{\frac{\rho}{M}} \sum_{i=1}^{P} \sum_{k'=0}^{N-1} \sum_{l'=0}^{M-1} h_{eq,i} g_i[k',l'] x[(k-k')_N, (l-l')_M] + v[k,l] \tag{4.7}$$

where $v[k,l] \sim \mathcal{CN}(0, \sigma_v^2)$ is additive noise and

$$h_{eq,i} = h_{0,i} h_i e^{-j2\pi\nu_i\tau_i}$$
$$g_i[k',l'] = \sum_{n=0}^{N-1} e^{-j2\pi nT(k'\Delta\nu - \nu_i)} \sum_{m=0}^{M-1} e^{j2\pi m\Delta f(l'\Delta\tau - \tau_i)}$$

The transmission power is divided by M since it is equally distributed among the M subcarriers that transmit simultaneously in a time slot T. The propagation delays and Doppler shifts do not correspond to integer positions in the delay-Doppler grid, therefore fractional delays and Doppler shifts appear (fractional delay - fractional Doppler) according to

$$\tau_i = \frac{l_{\tau_i} + \lambda_{\tau_i}}{M\Delta f}, \qquad \nu_i = \frac{k_{\nu_i} + \kappa_{\nu_i}}{NT}$$

In this case, l_{τ_i}, k_{ν_i} denote the integer delays, Doppler while $\lambda_{\tau_i}, \kappa_{\tau_i} \in (-0.5, 0.5]$ denote the fractional delays, Doppler. By substitution, $g_i[k,l]$ becomes

$$g_i[k',l'] = \sum_{n=0}^{N-1} e^{-j2\pi\frac{n}{N}(k'-k_{\nu_i}-\kappa_{\nu_i})} \sum_{m=0}^{M-1} e^{j2\pi\frac{m}{M}\Delta f(l'-l_{\tau_i}-\lambda_{\tau_i})} = \mathcal{F}\left(\frac{l'}{M\Delta f}, \tau_i\right) \mathcal{G}\left(\frac{k'}{NT}, \nu_i\right) \tag{4.8}$$

where $\mathcal{F}(\cdot), \mathcal{G}(\cdot)$ are the Dirichlet kernels defined in (3.35), (3.36). In the presence of fractional delays-Dopplers, the Dirichlet kernels do not vanish for any value of k', l'. Each symbol, that is, spreads its energy to all neighboring cells of the delay-Doppler grid. This spreading follows the sinc$(\cdot)$ function, that is, the proportion of scattered energy decreases as we move away from the symbol.

For this reason, the function $g[k',l']$ is computed only for $2E_\nu + 1$ values of k' and for $2E_\tau + 1$ values of l', such that $k' = k_{\nu_i} - p$, $-E_\nu \leq p \leq E_\nu$ and $l' = l_{\tau_i} - q$, $-E_\tau \leq q \leq E_\tau$. After simplifications, the final form of the input-output relationship can be written as

$$\hat{x}[k,l] = \sqrt{\frac{\rho}{M}} \sum_{i=1}^{P} \sum_{q=-E_\tau}^{E_\tau} \sum_{p=-E_\nu}^{E_\nu} \frac{h_{eq,i}}{NM} \frac{e^{-j2\pi(q+\lambda_{\tau_i})} - 1}{e^{-j\frac{2\pi}{M}(q+\lambda_{\tau_i})} - 1} \frac{e^{j2\pi(p+\kappa_{\nu_i})} - 1}{e^{j\frac{2\pi}{N}(p+\kappa_{\nu_i})} - 1}$$
$$\times x[(k - k_{\nu_i} + p)_N, (l - l_{\tau_i} + q)_M] + v[k,l] \tag{4.9}$$

The above relationship can be expressed in matrix form as

$$\hat{\mathbf{x}} = \sqrt{\frac{\rho}{M}} \mathbf{H}_{eq} \mathbf{x} + \mathbf{v} \tag{4.10}$$

where $\hat{\mathbf{x}} = \text{vec}(\hat{\mathbf{X}})$, $\mathbf{x} = \text{vec}(\mathbf{X})$, $\mathbf{v}$ is the $(1 \times NM)$ noise vector and

$$\mathbf{H}_{\mathbf{eq}} = \sum_{i=1}^{P} \frac{h_{eq,i}}{NM} \sum_{q=-E_\tau}^{E_\tau} \sum_{p=-E_\nu}^{E_\nu} \frac{e^{-j2\pi(q+\lambda_{\tau_i})} - 1}{e^{-j\frac{2\pi}{M}(q+\lambda_{\tau_i})} - 1} \frac{e^{j2\pi(p+\kappa_{\nu_i})} - 1}{e^{j\frac{2\pi}{N}(p+\kappa_{\nu_i})} - 1} \Pi_M^{l_{\tau_i}-q} \otimes \Pi_N^{k_{\nu_i}-p} \tag{4.11}$$

with Π_K being the $K \times K$ circular shift matrix and $\otimes$ being the Kronecker product.

The form of the equivalent channel matrix in (4.11) reveals that $\mathbf{H}_{eq}$ is a matrix consisting of circularly arranged blocks, where each block is also a circulant matrix (Block Circulant with Circulant Blocks - BCCB). Such matrices are diagonalized by the two-dimensional discrete Fourier transform (2D DFT) and therefore can be written as [6]

$$\mathbf{H}_{eq} = \mathbf{F}\mathbf{\Lambda}\mathbf{F}^H \tag{4.12}$$

where $\mathbf{F} = \mathbf{F}_M^H \otimes \mathbf{F}_N$ and $\mathbf{\Lambda} = \text{diag}\{\lambda_1, ...\lambda_{NM}\}$ with $\lambda_i, i = 1, ..., NM$ forming the eigenvalues of the equivalent channel matrix. For convenience in notation, $\tilde{\mathbf{H}}_{eq} = \sqrt{\frac{\rho}{M}}\mathbf{H}_{eq}$ and $\tilde{\mathbf{\Lambda}} = \sqrt{\frac{\rho}{M}}\mathbf{\Lambda}$ are defined, so that $\tilde{\mathbf{H}}_{eq} = \mathbf{F}\tilde{\mathbf{\Lambda}}\mathbf{F}^H$.

For this analysis, the first stage of detection is equalization with a low-complexity MMSE equalizer, whose transformation matrix is given as

$$\tilde{\mathbf{G}}_{\text{MSSE}} = \mathbf{F}(\tilde{\mathbf{\Lambda}}^*\tilde{\mathbf{\Lambda}} + \sigma_v^2\mathbf{I})^{-1}\tilde{\mathbf{\Lambda}}^*\mathbf{F}^H \tag{4.13}$$

The symbols received from the output of the equalizer are detected according to the decision rule of the selected constellation and subsequently the bit error probability can be calculated.

B. Transmission Rate Analysis

The output of the MMSE equalizer will be, according to the above analysis

$$\mathbf{y} = \tilde{\mathbf{G}}_{\text{MMSE}}(\tilde{\mathbf{H}}_{eq}\mathbf{x} + \mathbf{v}) = \mathbf{F}(\tilde{\mathbf{\Lambda}}^*\tilde{\mathbf{\Lambda}} + \sigma_v^2\mathbf{I})^{-1}\tilde{\mathbf{\Lambda}}^*\tilde{\mathbf{\Lambda}}\mathbf{F}^H\mathbf{x} + \mathbf{F}(\tilde{\mathbf{\Lambda}}^*\tilde{\mathbf{\Lambda}} + \sigma_v^2\mathbf{I})^{-1}\tilde{\mathbf{\Lambda}}^*\mathbf{F}^H\mathbf{v} \tag{4.14}$$

Therefore the signal-to-noise ratio for the (n, m) symbol will be

$$\gamma_{n,m} = \frac{|\tilde{\lambda}_{n,m}|^2}{\sigma_v^2} = \frac{P_t|\lambda_{n,m}|^2}{PM\Delta f N_0} \tag{4.15}$$

For the calculation of the achievable transmission rate it is taken into account that the OTFS waveform is implemented as an additional layer on top of existing OFDM systems. Therefore, when sending symbols within a time slot of duration T, a cyclic prefix of length L_{cp} is added, which handles intersymbol interference. Therefore, a penalty on the transmission rate is introduced which is defined as $\eta_{cp} = \frac{M}{M+L_{cp}}$. Finally, the achievable transmission rate after the MMSE equalizer is given as [7]

$$R = -\eta_{cp}B\log_2\left(\frac{1}{NM}\sum_{n,m}\frac{1}{1+\gamma_{n,m}}\right) \tag{4.16}$$

Particular interest is shown in the behavior of the achievable transmission rate when the number of antennas increases asymptotically to infinity. It can be shown that the eigenvalues of the matrix $\mathbf{H}_{eq}$ are equal to

$$\lambda_{n,m} = \sum_{i=1}^{P} h_{eq,i}e^{-j2\pi m\Delta f\tau_i}e^{j2\pi nT\nu_i} \tag{4.17}$$

(The complete mathematical proof of the above relationship is provided in Appendix A)

It is assumed that for adequate spatial separation of the antennas the paths arriving from them are statistically independent from each other. That is $\mathbb{E}[|\lambda|^2] = \sum_{i=1}^{P}\mathbb{E}[|h_{eq.i}|^2]$. Then, the average SNR will be

$$\bar{\gamma} = \frac{P_t\mathbb{E}[|\lambda|^2]}{PM\Delta f N_0} = \gamma_0\frac{1}{P}\sum_{i=1}^{P}\mathbb{E}[|h_{eq,i}|^2] = \frac{\gamma_0}{P}\sum_{i=1}^{P}\frac{\eta}{\|\psi_u - \psi_i^P\|} \tag{4.18}$$

where $\gamma_0 = \frac{P_t}{M\Delta f N_0}$. When the number of paths becomes large, then by the Central Limit Theorem the eigenvalue $\lambda_{n,m}$ results as a sum of a large number of independent variables and therefore its statistical distribution converges to Complex Gaussian ($\mathcal{CN}$). Then its magnitude follows a Rayleigh distribution, and its square follows an Exponential distribution. This means that the instantaneous value of the signal-to-noise ratio also follows an exponential distribution with mean value given by (4.18) and its probability density function is

$$f_\gamma(\gamma) = \frac{1}{\bar{\gamma}} e^{-\frac{\gamma}{\bar{\gamma}}} \tag{4.19}$$

Moreover, when the product NM takes large values, which is generally true, the Law of Large Numbers states that the sample mean of the quantity $\frac{1}{1+\gamma_{n,m}}$ will tend toward its statistical mean. That is

$$\frac{1}{NM} \sum_{n,m} \frac{1}{1+\gamma_{n,m}} \approx \mathbb{E}[\frac{1}{1+\gamma}] = \int_0^\infty \frac{1}{1+\gamma} \frac{1}{\bar{\gamma}} e^{-\frac{\gamma}{\bar{\gamma}}} \, d\gamma = \frac{1}{\bar{\gamma}} e^{\frac{1}{\bar{\gamma}}} E_1(\frac{1}{\bar{\gamma}}) \tag{4.20}$$

where $E_1(x)$ denotes the exponential integral function $E_1(x) = \int_x^\infty \exp(-t)/t \, dt$. The achievable transmission rate is, finally

$$\bar{R} = -\eta_{cp} B \log_2 \left(\frac{1}{\bar{\gamma}} e^{\frac{1}{\bar{\gamma}}} E_1(\frac{1}{\bar{\gamma}}) \right) \tag{4.21}$$

For $P \to \infty$, equation (4.18) becomes

$$\begin{aligned} \bar{\gamma}_\infty = \frac{\gamma_0 \eta}{P} \sum_{i=1}^{P} \frac{\eta}{(x_{p,i} - x_u)^2 + H^2} &\approx \frac{\gamma_0 \eta}{L} \int_0^L \frac{1}{(x - x_u)^2 + H^2} \, dx \\ &= \frac{\gamma_0 \eta}{LH} \left[\arctan\left(\frac{L - x_u}{H} \right) + \arctan\left(\frac{x_u}{H} \right) \right] \end{aligned} \tag{4.22}$$

and therefore

$$\bar{R}_\infty = -\eta_{cp} B \log_2 \left(\frac{1}{\bar{\gamma}_\infty} e^{\frac{1}{\bar{\gamma}_\infty}} E_1(\frac{1}{\bar{\gamma}_\infty}) \right) \tag{4.23}$$

Since the magnitude of the eigenvalues of the equivalent channel matrix is modeled to have a Rayleigh distribution, the worst case fading scenario, the result obtained from the above equation can serve as a lower bound on the channel performance. An upper bound on the capacity can be found using Jensen's inequality in (4.16), that is

$$R \leq \frac{1}{NM} \sum_{n,m} \eta_{cp} B \log_2(1 + \gamma_{n,m}) \leq \eta_{cp} B \log_2(1 + \bar{\gamma}) \tag{4.24}$$

Since $\log_2(x)$ is a concave function.

It is worth noting that the above relationships concern a specific position of the user.

4.2.3 Results and Discussion

The performance of the proposed OTFS modulation in PASS systems is evaluated through simulations. Specifically, it is assumed that the train moves along the x axis with constant velocity. The velocity of the train is significantly smaller than the information transmission speed, therefore at each position on the x axis the channel is considered invariant. The noise power is considered to be -90dBm, the operating frequency is $f_c = 5.9$GHz, the effective dielectric constant is $n_{eff} = 1.4$. The waveguide operates at a frequency well below the cutoff frequency, therefore the effective dielectric constant is considered constant and independent of frequency. The waveguide has length $L = 500$m and is placed at height $H = 5$m. Finally, the transmission of one OTFS frame occupies $N = 16$ time slots and $M = 512$ subcarriers with spacing $\Delta f = 30$kHz. The transmission power is $P_t = 20$dBm, unless otherwise stated. All the extracted metrics are computed over a set of points on the x axis and the spatial average is presented. The proposed system is compared with the OFDM waveform.

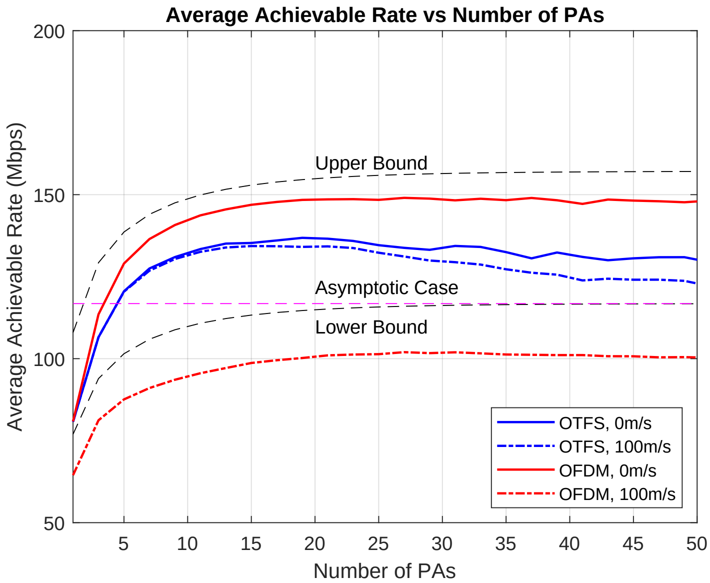

Figure 4.3: Average achievable transmission rate for various values of the number of PAs

First, the achievable transmission rate is studied for various values of the number of PAs, P. Figure 4.3 shows that initially the transmission rate increases as the number of antennas increases. Indeed, as the propagation paths increase, the average received power of the user also increases with respect to its positions. This occurs up to a point, after which the phases exhibit destructive interference. That is, as more propagation paths appear, the phases of the eigenvalues of the equivalent channel matrix are uniformly distributed over $[0, 2\pi]$ and therefore the channel tends to be a Rayleigh fading channel. Equations (4.21), (4.23) model the lower bound of channel performance, where it is assumed that fading is Rayleigh. For large values of P the central limit theorem begins to hold and therefore the average achievable transmission rate approaches asymptotically the lower bound. The upper bound given by (4.24) coincides with Shannon capacity. For small values of P where the channel benefits from multiple paths, the average achievable transmission rate approaches the upper bound. The difference observed by changing the velocity of the receiver is due to additional interference resulting from additional fractional Doppler. The OFDM waveform shows better performance when the receiver velocity is zero, as it is not affected by interference due to fractional delays. Nevertheless, with the appearance of Doppler, the OFDM subcarriers spread energy to adjacent subcarriers resulting in the appearance of significant inter-carrier interference (ICI) resulting in the average achievable transmission rate decreasing.

Henceforth, the number of antennas selected for the simulations is $N = 15$. Figure 4.4 shows the ability of OTFS to maintain a steady and high average achievable transmission rate even in environments where velocities, and thus Doppler shifts, are large. OFDM on the other hand deteriorates significantly.

Figure 4.5 reveals that in the OTFS waveforms and the OFDM waveform without Doppler, the

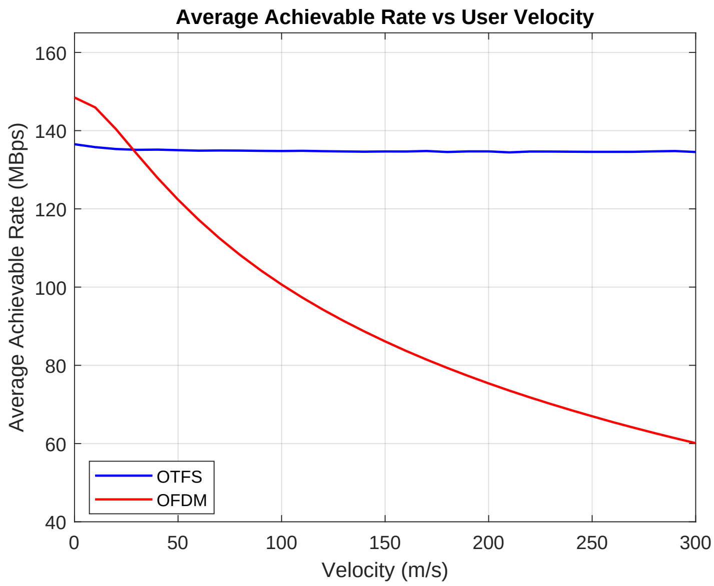

Figure 4.4: Average achievable transmission rate for various receiver velocities

average achievable transmission rate increases in the same way as the transmission power increases (the slopes of the curves are the same). In OFDM with Doppler present, as transmission power increases, so does the power of ICI interference. As a result, the average achievable transmission rate increases at a decreasing rate (the slope of the curve is decreasing).

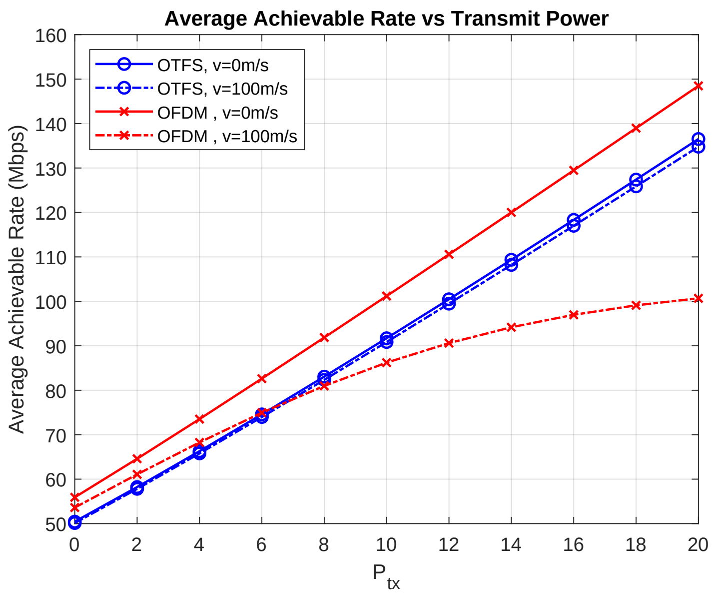

Figure 4.5: Average achievable transmission rate for various transmission power values

In Figure 4.6 the performance of the system in terms of bit error probability is shown. It is clear that the diversity offered by multiple propagation paths in the delay-Doppler domain makes the OTFS waveform particularly reliable in channels with double dispersion. With the appearance of Doppler phenomena, moreover, the discrete paths ”spread” in the delay-Doppler grid with the result that the interference energy due to fractional delays and Doppler is reduced and the error probability becomes smaller. On the other hand, the OFDM waveform has poor performance even in environments without Doppler. This happens because in OFDM the energy of symbols is not spread to all subcarriers (by some Fourier transform or precoder). Therefore, if a subcarrier is found in deep fading, then the information it carried is completely lost.

These results show that in PASS systems in applications with large relative velocities between transmitter and receiver, the OTFS waveform offers significant advantages. The average data transmission rate has stable behavior independent of Doppler shifts and over a wide range of transmission powers. The number of antennas can be selected so that full exploitation of the diversity offered by OTFS is achieved. Finally, the OTFS waveform offers high and stable performance regarding bit error probability even in the presence of Doppler.

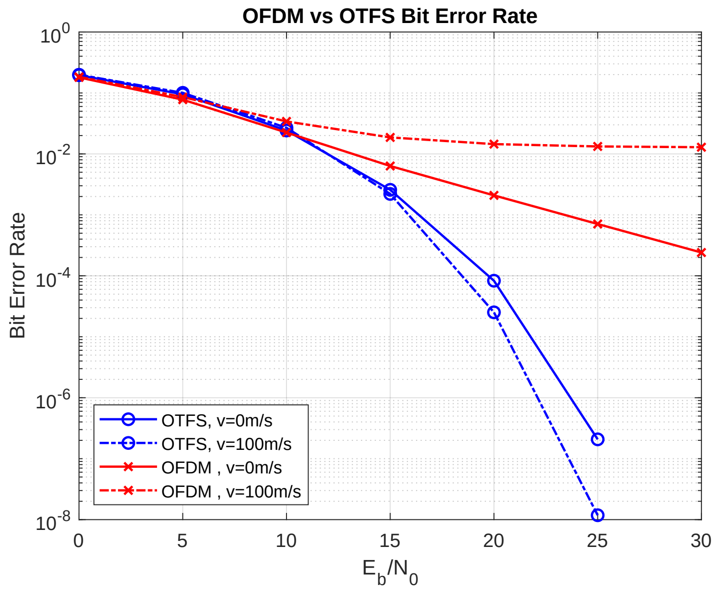

Figure 4.6: Average Bit Error Probability of OTFS-PASS

In conclusion, the above results reveal the clear superiority of the OTFS waveform compared to the corresponding OFDM in PASS systems, offering high and stable performance even in environments with pronounced Doppler phenomena. However, the practical implementation of such a system faces a significant limitation at the hardware level. As observed in Figure 4.7, which depicts the time domain representation of an OTFS frame, the generated signal is characterized by significant amplitude fluctuations. These sharp peaks translate into a high peak-to-average power ratio (PAPR). In practical communication systems, high PAPR drives power amplifiers into their non-linear region of operation, causing significant signal distortion and drastically complicating correct detection. Therefore, the need to manage this phenomenon is imperative. Toward this direction, modulation techniques are investigated which aim at reducing PAPR. In the next chapter, the PAPR of the OTFS waveform is studied in detail and the OTFS Constant Envelope (CE-OTFS) modulation technique is proposed, which achieves theoretically unity PAPR.

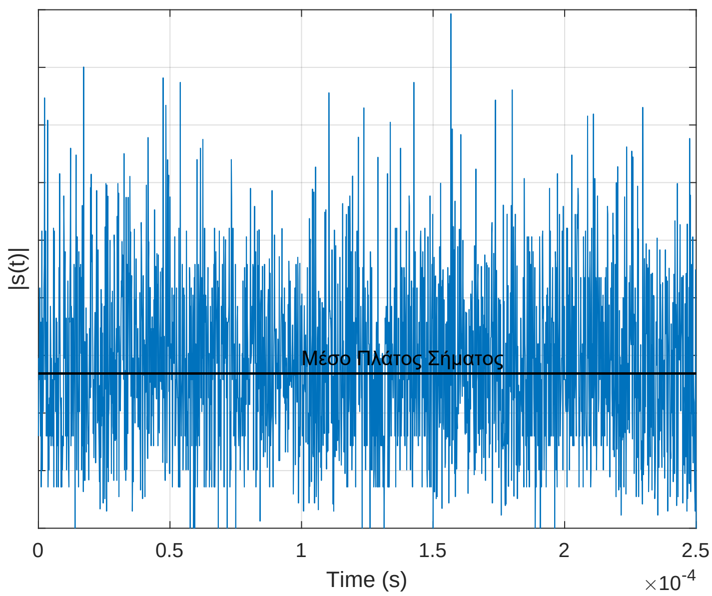

Figure 4.7: Time domain representation of the OTFS waveform

Chapter 5

OTFS Constant Envelope

Let a waveform $s(t)$ of duration T be transmitted from a transmitter and whose samples when sampled at rate $f_s = 1/T_s$ are $s[k] = s(kT_s), k = 0, ..., K$. Then the PAPR ratio is defined as

$$\text{PAPR} = \frac{\max_k\{|s[k]|^2\}}{\mathbb{E}[|s[k]|^2]} \tag{5.1}$$

In typical transceiver architectures, the signal undergoes amplification through power amplifiers before transmission. The power amplifiers are characterized by the characteristic curve of input power - output power shown in Figure 5.1. Three operating regions of a power amplifier can be distinguished:

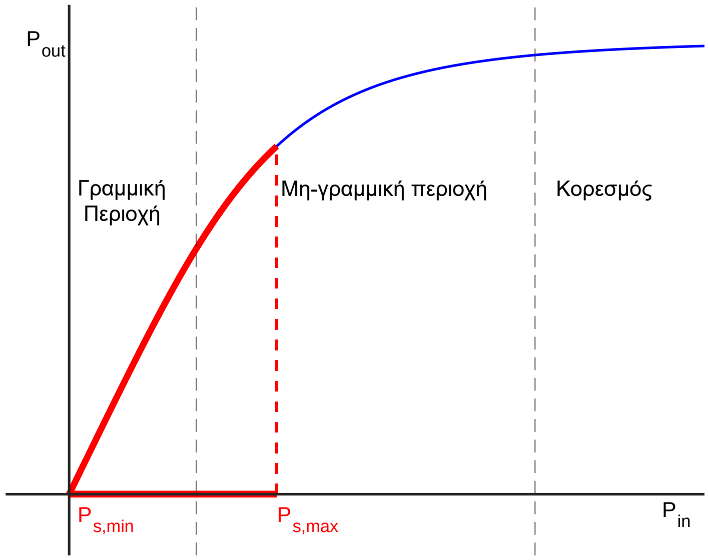

Figure 5.1: The characteristic curve of a power amplifier has three regions: linear, nonlinear, and saturation. As shown in the figure, if the power range of an input signal is sufficiently large, then the power amplifier may operate in the nonlinear region resulting in distorted output.

the linear region, the nonlinear region, and the saturation region. In the linear region, the input-output relationship is linear with gain coefficient G, i.e., $P_{out} = GP_{in}$. In the nonlinear region, the amplifier output does not increase linearly as the input increases, resulting in output compression. Finally, in the saturation region, the amplifier cannot further amplify the output signal and its output reaches a constant value P_{sat}. It is clear that if a signal has an amplitude with large variation, then the amplifier may be forced to operate in its nonlinear region and the resulting output signal will be distorted.

5.1 PAPR of OTFS

In the case of OTFS, the waveform is described by (3.18), has duration NT, and occupies bandwidth $M\Delta f$. The signal is sampled at rate $f_s = M\Delta f$ or at integer intervals $T_s = \frac{T}{M}$ and the samples obtained are

$$s[k] = s(kT_s) = s(k\frac{T}{M}) = \sum_{n'=0}^{N}\sum_{m'=0}^{M} X[n', m']g_{tx}(\frac{kT}{M} - n'T)e^{j2\pi m'\Delta f(\frac{kT}{M} - n'T)} \tag{5.2}$$

Or equivalently

$$s[k] = \sum_{n'=0}^{N}\sum_{m'=0}^{M} X[n', m']g_{tx}[k - n'M]e^{j2\pi\frac{m'}{M}(k-n'M)} \tag{5.3}$$

For the analysis, it is convenient to express the index k as a two-dimensional index decomposed as $k = m + nM$, so (5.3) can be written as

$$s[m+nM] = \sum_{n'=0}^{N}\sum_{m'=0}^{M} X[n', m']g_{tx}[m+(n-n)'M]e^{j2\pi\frac{m'}{M}(m+(n-n')M)} = \sum_{m'=0}^{M} X[n, m']e^{j2\pi\frac{m'm}{M}} \tag{5.4}$$

assuming that the pulse $g_{tx}(t)$ is rectangular with duration T. Therefore, the samples obtained can be represented through a matrix $\mathbf{S} \in \mathbb{C}^{N\times M}$ for which $S[n, m] = s(m + nM)$. It is observed that the rows of the matrix S constitute the inverse Fourier transform of the rows of the matrix of modulated symbols in the time-frequency domain $\mathbf{X}$, i.e.,

$$\mathbf{S} = \mathbf{X}\mathbf{F}_M^H \tag{5.5}$$

where $\mathbf{F}_K$ is the matrix of the discrete Fourier transform of K points. Following the same reasoning, it will hold for the modulated symbols in the time-frequency domain, according to (3.15), the relationship

$$\mathbf{X} = \mathbf{F}_N^H\boldsymbol{\mathcal{X}}\mathbf{F}_M \tag{5.6}$$

where the matrix $\boldsymbol{\mathcal{X}} \in \mathbb{C}^{N\times M}$ consists of $N \times M$ information symbols that belong to some constellation $\mathcal{A}$. In total, from (5.5), (5.6) we obtain

$$\mathbf{S} = \mathbf{F}_N^H\boldsymbol{\mathcal{X}} \tag{5.7}$$

The above analysis shows that the samples sent from the transmitter result from an inverse discrete Fourier transform applied to the information symbols. The phases of the symbols add both constructively and destructively resulting in the amplitudes of the samples showing significant fluctuations. For this reason, the OTFS waveform, like other multi-carrier waveforms, exhibits increased PAPR ratio. In fact, an upper bound of the PAPR of OTFS modulation can be found. The numerator in the relationship (5.1) is analyzed, using the Cauchy-Schwarz inequality, as

$$\begin{aligned}\max_k\{|s[k]|^2\} &= \max_{q,r}\{|s[r+qM]|^2\} = \max_{q,r}\{|\sum_{q'=0}^{N-1}\mathcal{X}[q', r]e^{j2\pi\frac{q'q}{N}}|^2\} \\ &\leq \max_{q,r}\{\sum_{q'=0}^{N-1}|\mathcal{X}[q', r]|^2\sum_{q'}^{N-1}|e^{j2\pi\frac{q'q}{N}}|^2\} \leq N^2\max_{c\in\mathcal{A}}\{|c|^2\}\end{aligned} \tag{5.8}$$

where $c \in \mathcal{A}$ are the symbols of the constellation $\mathcal{A}$. Regarding the denominator of (5.1), with the help of Parseval's theorem, we obtain

$$\mathbb{E}[|s[k]|^2] = N\mathbb{E}[|\mathcal{X}[q,r]|^2] = N\sigma_a^2 \tag{5.9}$$

where σ_a^2 is the average symbol energy of the constellation $\mathcal{A}$. Finally, (5.1) is bounded according to (5.8), (5.9):

$$\text{PAPR} \leq \frac{N \max_{c\in\mathcal{A}}\{|c|^2\}}{\sigma_a^2} \tag{5.10}$$

It is worth noting that unlike other multi-carrier modulation techniques, the upper bound of PAPR of OTFS increases linearly as a function of the number of time slots, N, and not the number of subcarriers, M. In practice, N is usually smaller than M, so OTFS is expected to have lower PAPR than other modulations, such as OFDM for example. To show this, the Complementary Cumulative Distribution Function (CCDF) is calculated for the two waveforms, which is defined as

$$\text{CCDF}(\gamma_0) = \text{Pr}(\text{PAPR} > \gamma_0) \tag{5.11}$$

for various values of N, M. Figures 5.2 and 5.3 show that, indeed, in each case OTFS has lower PAPR than OFDM, given that $N < M$. It is also seen that the PAPR of OTFS varies significantly as N varies while for variations of M, its behavior remains relatively the same. The reverse is observed for the PAPR of the OFDM waveform. The above diagrams were created using OTFS and OFDM

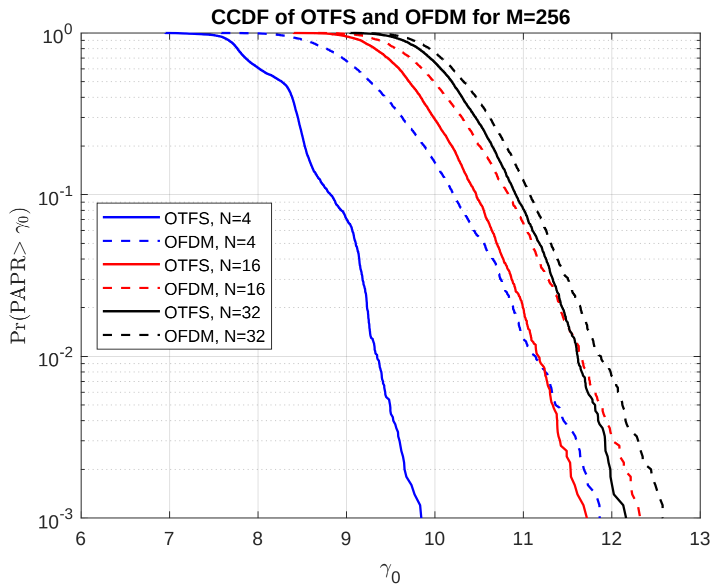

Figure 5.2: CCDF of OTFS, OFDM for constant M. As N increases, the CCDF curves of OTFS change significantly. The behavior of the OFDM waveform changes much less.

waveforms for various values of N, M. The transmit pulses are rectangular, sampling is done at the Nyquist rate, while the samples pass through a raised cosine filter with coefficient $\beta = 0.5$, to achieve oversampling with oversampling ratio $Q = 4$.

5.2 Constant Envelope (CE) - OTFS

Improving the PAPR of the OTFS waveform is an active research field. Various PAPR reduction techniques have been proposed in the literature, concerning the use of companders [8], [9], pre-coders

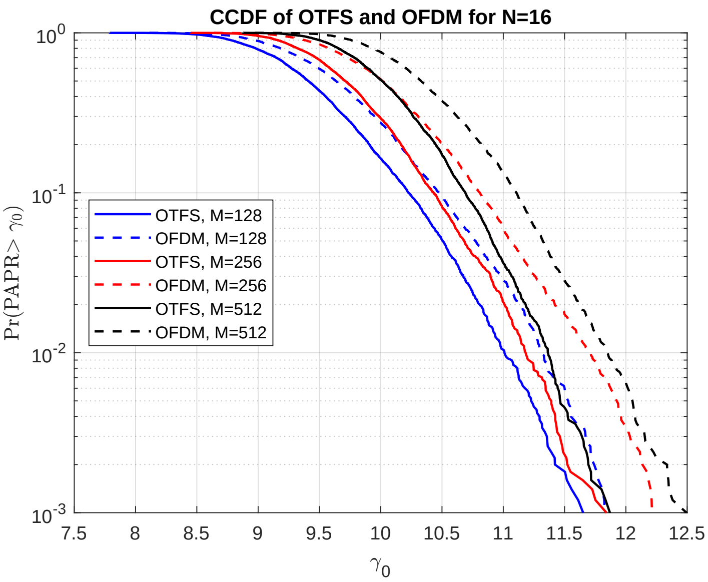

Figure 5.3: CCDF of OTFS, OFDM for constant N. As M increases, the CCDF curves of OFDM change significantly. The behavior of the OTFS waveform changes to a smaller degree.

[10], [11], [12], peak windowing techniques [13], as well as techniques based on iterative minimization algorithms [14], [15]. Although all the aforementioned techniques achieve better levels of PAPR, these may remain high resulting in distortion continuing to be observed at the output of a power amplifier. In this section, therefore, a Constant Envelope (CE) - OTFS modulation technique is proposed which achieves a unity PAPR ratio in each sequence of symbols transmitted by a transmitter.

5.2.1 Analysis of CE-OTFS Modulation

Let a telecommunications system which has N time slots of duration T and M subcarriers of bandwidth Δf, where $\mathcal{A}$ is the alphabet of a constellation of symbols. OTFS modulation can transmit, in each transmission, an $N \times M$ grid of symbols, according to equation (5.7). To achieve a unity PAPR ratio, the transmitted signal must be phase modulated. Therefore, the samples in (5.7) must be purely real numbers. It is observed that the symbol matrix **S** coincides with the information matrix **X**, if the inverse discrete Fourier transform is applied to each column of it. For the elements of **S** to be real, each column of it must be of the following form, so that the properties of Hermitian symmetry are exploited:

$$\mathbf{x}_m = [0, \mathcal{X}_l[1], \mathcal{X}_l[2], ..., \mathcal{X}_l[N_s], \mathbf{0}_{1\times N_{zp}}, 0, \mathcal{X}_l^*[N_s], ..., \mathcal{X}_l^*[2], \mathcal{X}_l^*[1]]^T, \quad m = 1, ..., M$$

where $\{\mathcal{X}[i]\}_{i=1}^{N_s}, \mathcal{X}[i] \in \mathcal{A}$ are the information symbols and $\mathbf{0}_{1\times N_{zp}}$ is a row vector consisting of N_{zp} zeros [16]. This vector serves to oversample the information symbols, which facilitates their correct detection by a phase detector. Additionally, we must have $N = 2N_s + N_{zp} + 2$. In this case, the oversampling ratio is defined as

$$Q \equiv \frac{N}{N - N_{zp}} \tag{5.12}$$

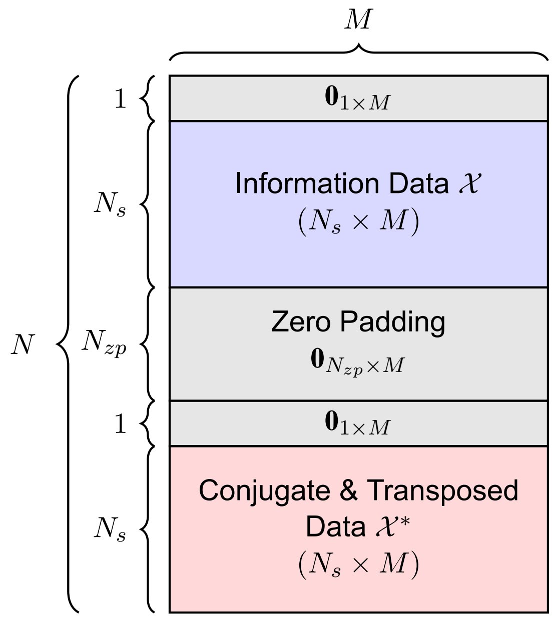

Figure 5.4: Structure of matrix **S**. Hermitian symmetry serves to produce a purely real signal after processing of the matrix by the OTFS modulator

For the sum with respect to N, on the m-th column of the information matrix, it will hold, according to (3.15)

$$\begin{aligned}\sum_{k=0}^{N-1} x_m[k] e^{j2\pi \frac{nk}{N}} &= 2\sum_{k=1}^{N_s}\left(\Re\{\mathcal{X}_m[k]\}\cos\left(\frac{2\pi nk}{N}\right) - \Im\{\mathcal{X}_m[k]\}\sin\left(\frac{2\pi nk}{N}\right)\right)\\ &= 2\sum_{k=1}^{2Ns} I_m[k] q_n[k] \end{aligned} \tag{5.13}$$

where

$$I_m[k] = \begin{cases} \Re\{\mathcal{X}_m[k]\}, & k = 1, 2, ..., N_s \\ -\Im\{\mathcal{X}_m[k-N_s]\}, & k = N_s + 1..., 2N_s \end{cases}$$

$$q_n[k] = \begin{cases} \cos\left(\frac{2\pi nk}{N}\right), & k = 1, 2, ..., N_s \\ \sin\left(\frac{2\pi n(k-N_s)}{N}\right), & k = 1, ..., 2N_s \end{cases}$$

Equation (5.7), finally, gives the samples of the modulator output signal

$$S[n, m] = \frac{2}{\sqrt{N}} \sum_{k=1}^{2N_s} I_m[k] q_n[k] \tag{5.14}$$

where C is a real constant, which are purely real numbers. The baseband signal can be written as

$$m(t) = C_{norm} \sum_{n=0}^{N-1}\sum_{m=0}^{M-1} S[n, m] p\left(t - nT - \frac{mT}{M}\right) \tag{5.15}$$

where $C_{norm} = \sqrt{\frac{N}{2N_s\sigma^2}}$, $\sigma^2 = \mathbb{E}[|\mathcal{X}[k, l]|^2]$ is the signal amplitude normalization constant and $p(t)$ is the rectangular pulse of duration $\frac{T}{M}$. The signal that is finally transmitted has the form

$$s(t) = Ae^{j\phi(t)} \tag{5.16}$$

where A is the amplitude of the carrier and

$$\phi(t) = 2\pi h m(t) \tag{5.17}$$

with h being the modulation index. If the signal $s(t)$ is sampled at intervals $Ts = \frac{T}{M}$ (Nyquist sampling), then for the samples we have $\mathbb{E}[|s|^2] = \max\{|s|^2\} = A^2$ and therefore PAPR=1, where $s[n,m] = A\exp(-j2\pi h S_0[n,m])$.

5.2.2 CE-OTFS in AWGN Channel

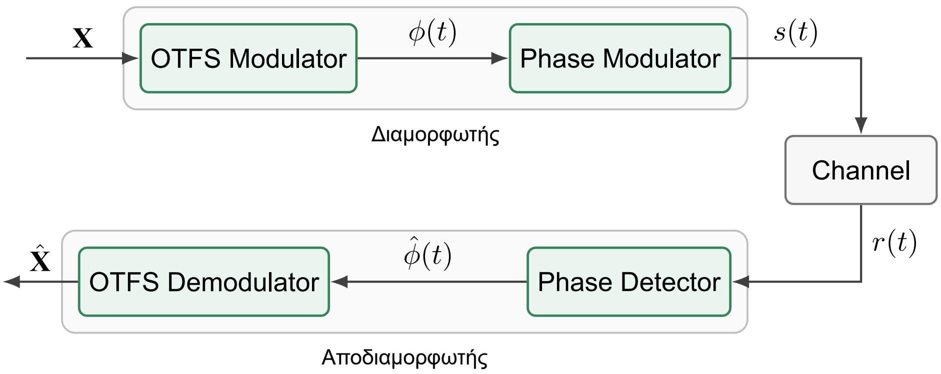

Figure 5.5: Block diagram of modulator/demodulator of CE-OTFS waveform

For the analysis, it will be assumed that the constellation used for modulating the information is the normalized Λ-QAM. According to (3.19), for the AWGN channel, where $h(\tau,\nu) = \delta(\tau)$, the received signal will be

$$r(t) = s(t) + w(t) \tag{5.18}$$

where $w(t)$ is the additive noise, for whose samples we have $w[k,l] \sim \mathcal{CN}(0,\sigma_w^2)$. The signal is sampled and its phase is demodulated, resulting in obtaining the samples

$$\hat{\phi}[n,m] = \phi[n,m] + \theta_0 + \xi[n,m] \tag{5.19}$$

where θ_0 is the phase offset introduced by the phase detector and, if the noise is expressed as $w[n,m] = A_w\exp(j\phi_w)$, then

$$\xi[n,m] = \arctan\left(\frac{A_w[n,m]\sin(\phi_w[n,m] - \phi[n,m] - \theta_0)}{A + A_w[n,m]\sin(\phi_w[n,m] - \phi[n,m] - \theta_0)}\right) \tag{5.20}$$

Under high Carrier to Noise Ratio (CNR) conditions, the samples $\xi[n,m]$ can be considered statistically independent and follow a normal distribution with zero mean and variance $\sigma_\xi^2 = \frac{\sigma_w^2}{A^2}$. For the detection of information symbols, the receiver first must apply the discrete Fourier transform to the columns of the matrix of the phase samples of the received signal. That is

$$\hat{X}[k,l] = \frac{1}{\sqrt{N}}\sum_{k=0}^{N-1}\left(2\pi h C_{norm} S[n,l] + \theta_0 + \xi[n,l]\right)e^{-j2\pi\frac{nk}{N}} \tag{5.21}$$

The first term of (5.21) gives $2\pi h C_{norm} X[k,l]$ since it is the discrete Fourier transform (DFT) of the samples of the output of the inverse discrete Fourier transform in (5.7), the second term gives

$\sqrt{N}\theta_0\delta[k]$ (due to the DFT over a constant) and the third term is the noise $v[k,l]$, whose statistics do not change, since the discrete Fourier transform preserves the signal energy, i.e., $v[k,l] \sim \mathcal{CN}(0, \frac{\sigma_w^2}{A^2})$. It is worth noting that the phase offset introduced by the phase detector affects only the symbols in the first row of the matrix **X**. The first row, however, of the matrix is zero and does not contain any information symbol, due to its special structure. The information symbols are generally unaffected by constant phase errors. Finally, the input-output relationship is shaped as

$$\hat{X}[k,l] = 2\pi h C_{norm} X[k,l] + v[k,l] \tag{5.22}$$

where $k = 1, ..., N_s$, $l = 0, ..., M-1$

The bit error probability, when using Λ-QAM modulation with Gray coding and under high CNR conditions, can be approximated as

$$P_b \approx \frac{4}{\log_2 \Lambda}\left(1 - \frac{1}{\sqrt{\Lambda}}\right) Q\left(\sqrt{\frac{3\gamma}{\Lambda^2 - 1}}\right) \tag{5.23}$$

where

$$\gamma = (2\pi h)^2 \log_2 \Lambda \frac{E_b}{N_0} \tag{5.24}$$

$$E_b = \frac{A^2 NT}{MN_s \log_2 \Lambda} \tag{5.25}$$

with E_b the energy per bit. The expression of γ shows that as the modulation index h increases, the signal-to-noise ratio improves and the system is expected to have better performance. Nevertheless, for large values of h the phase of the signal may fall outside the limits $[-\pi, \pi)$.

The modulated signal $m(t)$ is the sum of independent and identically distributed random variables with zero mean and unit variance, therefore according to the Central Limit Theorem, $m(t) \sim \mathcal{N}(0,1)$. Consequently, the phase of the signal also follows a normal distribution $\phi(t) \sim \mathcal{N}(0, (2\pi h)^2)$. The probability that the phase falls outside the range $[-\pi, \pi]$ is given as

$$\mathrm{Pr}_{wrap} = \mathrm{Pr}\{\phi(t) < -\pi \text{ or } \phi(t) > \pi\} = 2Q(\frac{1}{2h})$$

Then an phase error is added to (5.19) which will equal $\Delta\phi[n,m] = \pm\pi$. The $\Delta\phi$ is a random variable with mean 0 and variance $\sigma_{\Delta\phi}^2 = (2\pi)^2 Pr_{wrap} = 8\pi^2 Q(\frac{1}{2h})$. In other words, there is now an additional noise factor in the signal-to-noise ratio, which is shaped as

$$\gamma_{eff} = \frac{\sigma_{\mathcal{X}}^2}{\sigma_\xi^2 + \sigma_{\Delta\phi}^2} = \frac{1}{\frac{1}{\gamma} + \frac{1}{\gamma_{\text{wrap}}}} \tag{5.26}$$

where

$$\gamma_{\text{wrap}} = \frac{(2\pi h C_{norm})^2}{8\pi^2 Q(1/(2h))} = \frac{Nh^2}{4N_s Q(1/(2h))} \tag{5.27}$$

The last relationship reveals the usefulness of oversampling: For a given number of symbols to be transmitted, a larger oversampling ratio Q increases the size of the vector $\mathbf{0}_{1\times N_{zp}}$ and consequently N. Thus, γ_{wrap} becomes smaller and the phase distortion has less catastrophic consequence on the error probability. This is justified by the fact that the larger N is, the energy of the distortion error is shared through the DFT among more symbols. As a result, the fraction of error energy added to the useful information symbols is smaller. The expression of the error probability becomes, finally,

$$P_b \approx \frac{4}{\log_2 \Lambda}\left(1 - \frac{1}{\sqrt{\Lambda}}\right) Q\left(\sqrt{\frac{3\gamma_{eff}}{\Lambda^2 - 1}}\right) \tag{5.28}$$

5.2.3 Results and Discussion

The performance of the CE-OTFS waveform is examined with total frame size $N = 32$, $M = 128$, oversampling coefficient $Q = 4$, and 16-QAM constellation. In the figure 5.6 it is confirmed that the PAPR of the waveform will be equal to unity, as expected since it is a phase modulation technique. The waveform is then simulated in the AWGN channel and the error probability is studied. In Figure

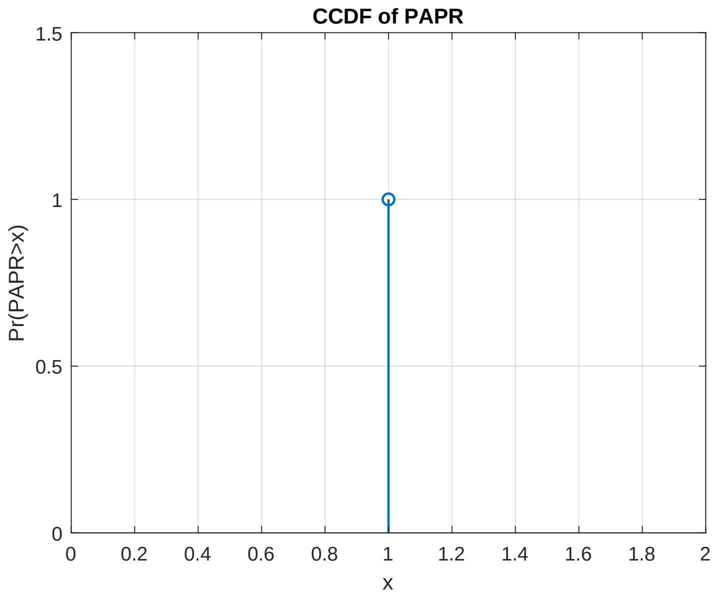

Figure 5.6: CCDF of PAPR of CE-OTFS waveform

5.7, it is shown that for small values of the modulation index h, the waveform shows satisfactory performance regarding error probability. In fact, as the modulation index increases, the power of the demodulated symbols increases in relation to the noise power resulting in a decrease in error probability. However, the analysis showed that the modulation index cannot increase arbitrarily. This

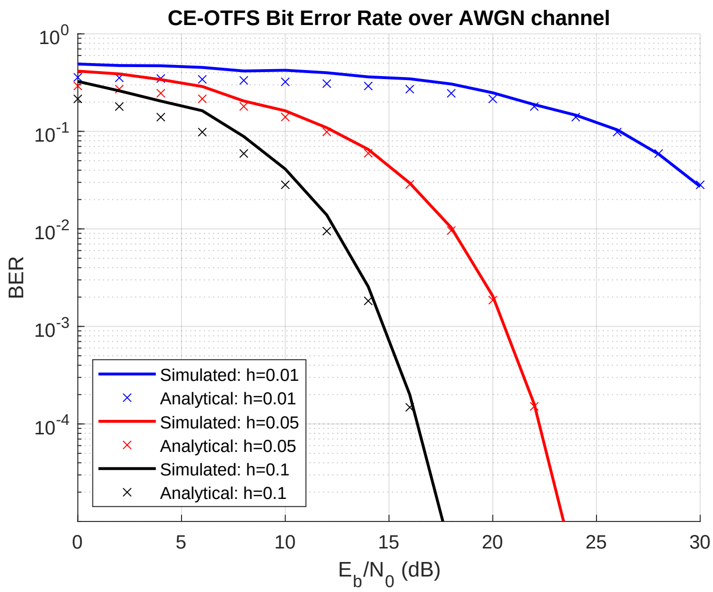

Figure 5.7: Error probability for small values of modulation index

fact is also confirmed by Figure 5.8, where it is shown that if h exceeds a critical value, then the errors resulting from the phase distortion in the phase detector exceed the number of errors due to thermal noise. For this reason, a lower bound also appears in the error probability of the system, which is worsened by further increase of the modulation index. The CE-OTFS waveform achieves a unity PAPR ratio regardless of the choice of its parameters. The variation of the parameters allows for control of the waveform behavior regarding e.g. the probability of errors. A major disadvantage

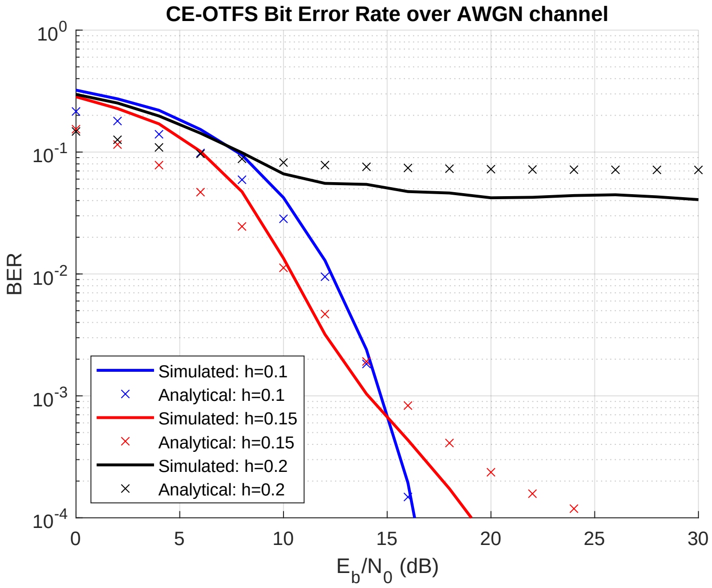

Figure 5.8: Error probability for large values of modulation index

of the CE-OTFS waveform is the inefficient exploitation of available resources. As mentioned at the beginning of the analysis, each subcarrier of the system can transmit over N time slots. Of these, only N_s are used for transmitting useful information, while the rest help achieve the desired characteristics of the waveform. In general terms, the ratio $N_s/N \approx \frac{2}{Q}$ is small. Furthermore, the phase distortion introduced by the phase detector creates the need for designing more optimal detectors that introduce additional complexity in the study of the waveform.

Chapter 6

Conclusions and Future Extensions

6.1 Conclusions

In this thesis, the Orthogonal Time Frequency Space (OTFS) modulation has been thoroughly investigated, establishing itself as one of the most promising technologies for future wireless networks (6G), especially in doubly dispersive channel environments. The thesis focused on two key aspects of OTFS modulation: its application to Pinching Antenna Systems (PASS) for high-speed train communications, and addressing the high Peak-to-Average Power Ratio (PAPR).

Regarding the first aspect, we analyzed the application of OTFS waveforms in PASS systems within tunnels to serve moving trains. An analytical mathematical model of the channel in the delay-Doppler domain was developed in the presence of fractional delays and Doppler. Simulation results showed that OTFS-PASS exploits the diversity offered by multiple PA antennas, maintaining high and stable achievable transmission rates even at very high speeds, in contrast to OFDM waveforms which collapse due to inter-carrier interference (ICI). We also proved asymptotically that, due to uncontrolled phase interference, if the number of antennas increases excessively, the channel tends toward the worst Rayleigh fading conditions, setting a lower limit on system capacity. Finally, we observed that OTFS waveforms suffer from high PAPR.

In the second aspect, we analytically demonstrated that OTFS modulation exhibits significant power fluctuations, leading to high PAPR. To address this problem, we proposed a novel constant envelope modulation architecture (CE-OTFS). Simulation results confirmed that the CE-OTFS technique achieves exactly unitary PAPR, preventing any distortion due to power amplifier nonlinearity. However, we found that for large values of the CE-OTFS modulation index, phase wrapping phenomena occur, which causes an error floor in system performance over AWGN channels.

6.2 Future Extensions

This thesis establishes strong foundations for optimizing high mobility systems, while simultaneously identifying areas of particular research interest.

6.2.1 Extensions to OTFS-PASS

The analysis of the achievable transmission rate of OTFS-PASS systems showed that there is a dependency on the number of antennas the system possesses. Therefore, a method for dynamic antenna selection based on receiver position could be examined to serve it optimally.

OTFS-PASS is a multi-carrier modulation technique and can be extended to multi-user downlink environments. It is important to investigate methods that optimally share available resources to achieve reliable, secure, and efficient service.

6.2.2 Extensions to CE-OTFS

A significant problem that emerged during CE-OTFS analysis is phase modulation distortion (wrapping). Advanced phase detectors that account for the statistics of symbols to be transmitted can thus be studied to identify errors resulting from such distortion and correct them.

Another negative characteristic of CE-OTFS is low spectral efficiency. A study of the information matrix structure could be conducted to ensure better spectral efficiency while maintaining correct symbol detection from the phase detector.

The study conducted addressed the AWGN channel and can be extended to analyze the CE-OTFS waveform in doubly dispersive channels.

Appendix A

Proofs

Proof of (4.17)
The channel in the time-frequency domain is given by the two-dimensional discrete Fourier transform of the channel in the delay-Doppler domain, that is

$$h(t,f) = \int\int h_c(\tau,\nu)e^{-j2\pi f\tau}e^{j2\pi\nu t}\,d\tau d\nu$$

Therefore

$$h(t,f) = \sum_{i=1}^{P} h_{eq,i}e^{-j2\pi f\tau_i}e^{j2\pi t\nu_i}$$

The channel response on the time-frequency domain is given by sampling $h(t,f)$ at integer multiples of $T, \Delta f$, that is:

$$H_{TF}[n,m] = h(t,f)|_{t=nT,f=m\Delta f} = \sum_{i=1}^{P} h_{eq,i}e^{-j2m\Delta f\tau_i}e^{j2\pi nT\nu_i}$$

Thus $\hat{X}_{TF}[n,m] = H_{TF}[n,m]X_{TF}[n,m] + w[n,m]$. The equivalent channel matrix, that is, will be diagonal and its eigenvalues will equal the samples $H[n,m]$.

The two-dimensional discrete Fourier transform is a unitary transform and preserves the eigenvalues of the matrix to which it is applied. Therefore, the eigenvalues of the equivalent channel in the delay-Doppler domain and in the time-frequency domain will coincide. Therefore,

$$\lambda_{n,m} = \sum_{i=1}^{P} h_{eq,i}e^{-j2\pi m\Delta f\tau_i}e^{j2\pi nT\nu_i}$$

which completes the proof ■

Bibliography

[1] R. Hadani et al., “Orthogonal time frequency space modulation”, in *2017 IEEE wireless communications and networking conference (WCNC)*, IEEE, 2017, pp. 1–6.

[2] A. Fukuda, H. Yamamoto, H. Okazaki, Y. Suzuki, and K. Kawai, “Pinching antenna: Using a dielectric waveguide as an antenna”, *NTT DOCOMO Technical J.*, vol. 23, no. 3, pp. 5–12, 2022.

[3] Y. Liu et al., “Pinching-antenna systems (pass): A tutorial”, *IEEE Transactions on Communications*, 2026.

[4] S. K. Mohammed, R. Hadani, A. Chockalingam, and R. Calderbank, “Otfs—a mathematical foundation for communication and radar sensing in the delay-doppler domain”, *IEEE BITS the Information Theory Magazine*, vol. 2, no. 2, pp. 36–55, 2022.

[5] Z. Ding, R. Schober, and H. V. Poor, “Flexible-antenna systems: A pinching-antenna perspective”, *IEEE Transactions on Communications*, 2025.

[6] G. Surabhi and A. Chockalingam, “Low-complexity linear equalization for otfs modulation”, *IEEE communications letters*, vol. 24, no. 2, pp. 330–334, 2019.

[7] E. N. Onggosanusi, A. G. Dabak, T. Schmidl, and T. Muharemovic, “Capacity analysis of frequency-selective mimo channels with sub-optimal detectors”, in *2002 IEEE International Conference on Acoustics, Speech, and Signal Processing*, IEEE, vol. 3, 2002, pp. III–2369.

[8] H. Bitra, P. Ponnusamy, S. Chintagunta, and S. Pragadeshwaran, “Nonlinear companding transforms for reducing the papr of otfs signal”, *Physical Communication*, vol. 53, p. 101 729, 2022.

[9] H. Bitra, P. Ponnusamy, and S. Chintagunta, “Reduction of papr in otfs using normalized μ-law and a-law companding transform”, *Internet Technology Letters*, vol. 5, no. 3, e344, 2022.

[10] M. N. Hossain, Y. Sugiura, T. Shimamura, and H.-G. Ryu, “Dft-spread otfs communication system with the reductions of papr and nonlinear degradation”, *Wireless Personal Communications*, vol. 115, no. 3, pp. 2211–2228, 2020.

[11] Y. Wu, C. Han, and T. Yang, “Dft-spread orthogonal time frequency space modulation design for terahertz communications”, in *2021 IEEE Global Communications Conference (GLOBECOM)*, IEEE, 2021, pp. 01–06.

[12] Y. I. Tek and E. Basar, “Papr reduction precoding for orthogonal time frequency space modulation”, in *2023 46th International conference on telecommunications and signal processing (TSP)*, IEEE, 2023, pp. 172–176.

[13] H. Shang et al., "Otfs modulation and papr reduction for iot-railways", *China Communications*, vol. 20, no. 1, pp. 102–113, 2023.

[14] A. S. Sümer, T. Yılmaz, E. Memişoğlu, and H. Arslan, "Exploiting otfs frame structure for papr reduction", in *2022 IEEE 96th Vehicular technology conference (VTC2022-Fall)*, IEEE, 2022, pp. 1–5.

[15] M. Sheikh-Hosseini and M. Uysal, "Design of a linear precoder for papr reduction of the otfs scheme in high mobility environments", *IEEE Transactions on Vehicular Technology*, 2025.

[16] S. C. Thompson, A. U. Ahmed, J. G. Proakis, J. R. Zeidler, and M. J. Geile, "Constant envelope ofdm", *IEEE transactions on communications*, vol. 56, no. 8, pp. 1300–1312, 2008.